Eur. Phys. J. C (2023) 83:342
https://doi.org/10.1140/epjc/s10052-023-11461-7

THE EUROPEAN PHYSICAL JOURNAL C

Regular Article - Theoretical Physics

Riding the Seesaw: what Higgsstrahlung may reveal about massive neutrinos

Tobias Felkl[a], **Adam Lackner**[b], **Michael Schmidt**[c]

Sydney Consortium for Particle Physics and Cosmology, School of Physics, The University of New South Wales, Sydney, NSW 2052, Australia

Received: 11 January 2023 / Accepted: 31 March 2023 / Published online: 28 April 2023

Abstract We investigate if the projected high-precision measurements of the cross section of the Higgsstrahlung process $e^+e^- \to Zh$ at a future electron–positron collider can be utilised to indirectly probe the fermionic Seesaw models. We consider the two centre-of-mass energies $\sqrt{s} = 240\,\text{GeV}$ and $365\,\text{GeV}$, and compare the collider reaches to constraints from electroweak observables, probes of lepton flavour universality and the existing and prospective bounds from searches for lepton flavour violation. For the analysis we assume the limit of an exactly conserved lepton-number symmetry. We find that while any appreciable correction to the Higgsstrahlung cross section is already strictly constrained in the Type-I Seesaw model, effects of up to $\mathcal{O}(10\%)$ are possible within Type-III Seesaw.

1 Introduction

Upon the discovery of the Higgs boson in 2012 [1,2], the particle content as proposed within the Standard Model (SM) was confirmed to exist. Precise determinations of the properties of the Higgs boson, as well as in other sectors of physics, are a major component of the proposed program of next-generation lepton colliders. There are five proposals for so-called electron–positron "Higgs factories" [3]: the Circular Electron Positron Collider (CEPC) [4–6], the International Linear Collider (ILC) [7–10], the Future Circular Collider (FCC-ee) [11–14], the Compact Linear Collider (CLIC) [15–17] and the Cool Copper Collider (C^3) [18–20]. The designation "Higgs factory" mainly refers to the stage of a future e^+e^- collider being run at a centre-of-mass energy of roughly $\sqrt{s} = 240$–$250\,\text{GeV}$, where the integrated cross section of the Higgsstrahlung process peaks and so dominates over all Higgs production mechanisms. Other stages involve the operation as a "Z factory" at the Z pole for $\sqrt{s} = m_Z$, close to the W^+W^- production threshold at $\sqrt{s} = 2m_W$, and close to or at the $t\bar{t}$ threshold for $\sqrt{s} = 350$–$370\,\text{GeV}$, as well as potential upgrades for runs at even higher centre-of-mass energies [21].

The incompleteness of the SM has been corroborated upon the measurement of neutrino oscillations by the Super-Kamiokande [22] and SNO collaborations [23,24], which evidence the need to introduce new physics in order to account for neutrino masses. A particularly straightforward way to do so is via postulating the existence of *sterile neutrinos*, several searches for which at future lepton colliders have been proposed. Most of the sensitivity studies focus on direct production of sterile neutrinos in electroweak processes and Higgs production [25–33], see also Refs. [34–37] for reviews on heavy neutral leptons at colliders. Similarly, electroweak triplet fermions at colliders have been studied in, e.g., Refs. [38,39]. The anticipated high precision attainable at future lepton colliders also serves as a motivation to consider virtual corrections, see e.g. Ref. [40]. In Refs. [41,42], the contribution of sterile neutrinos to the triple-Higgs coupling was studied.

In this work, we investigate the potential of electron–positron colliders to test the fermionic Seesaw scenarios [43–48], given the sub-percent precision to which these colliders are projected to measure the cross section of the Higgsstrahlung process $e^+e^- \to Zh$. Achieving this precision is possible due to the so-called "recoil method" that refers to the selection of Higgsstrahlung events solely through measuring the four-momenta of the decay products of the Z boson which recoils against the Higgs boson. This method is in principle applicable for any Higgs decay mode and thus allows for a model-independent reconstruction of the Higgs-boson mass, see for instance Ref. [3]. The Higgsstrahlung process is also well-understood in the SM. Recently, two-loop elec-

[a] e-mail: t.felkl@unsw.edu.au (corresponding author)
[b] e-mail: a.lackner@unsw.edu.au
[c] e-mail: m.schmidt@unsw.edu.au

troweak corrections to the SM cross section were calculated in Refs. [49,50]; see also Refs. [51–57].

We consider the process at two benchmark centre-of-mass energies, $\sqrt{s} = 240\,\text{GeV}$ and $365\,\text{GeV}$. As argued for in Ref. [58], the smaller cross section at larger s can be partly compensated for by a higher instantaneous luminosity which scales approximately linearly with s. Moreover, the additional boost of the Z and h bosons allows for a better separation of the respective jets and therefore a more precise measurement of $\sigma_{Zh} \times \text{BR}(H \to X)$. Further advantages mentioned are the immediate access to top-pair production as well as the $e^+e^- \to H\nu_e\overline{\nu_e}$ process via W^+W^- fusion which enables a precise determination of the Higgs-boson width, and the possibility to measure the Higgs-boson mass with a precision similar to the one at $\sqrt{s} = 240\,\text{GeV}$.

In the fermionic Seesaw models, the smallness of the absolute mass scale of the light neutrinos generically requires the neutrino Yukawa couplings to be tiny for TeV-scale sterile states, and consequently lepton-number conserving processes are suppressed [59–61] and beyond the reach of the proposed lepton colliders. In contrast, *symmetry-protected Seesaw models* [59,62–72] offer the possibility to entertain relatively light singlets or triplets around the TeV scale without the need to assume tiny Yukawa couplings only. Essentially, the new interaction states are assigned units of lepton number such that it is (approximately) conserved, which implies that some elements of the Dirac and Majorana mass matrices can be sizeable, whereas the remaining ones must be comparatively suppressed. The smallness of active neutrino masses is then guaranteed via the proportionality to these small entries, and does not only rely on an overall suppression through the large mass scale. In addition, no fine-tuned cancellation between (a priori unrelated) elements of the mass matrices are needed.

The remaining paper is organised as follows. In Sect. 2 we introduce the relevant theoretical framework. We discuss Higgsstrahlung and other relevant processes which are sensitive to the same parameters in Sect. 3. Our results are summarised and conclusions are drawn in Sect. 4. In the Appendices, more technical details and useful formulae are collected.

2 Theory framework

Firstly, to set our conventions for notation, signs, and normalisation, we state the electroweak (EW) and leptonic parts of the SM Lagrangian:

$$\begin{aligned}\mathcal{L}_{\text{EW}} = &-\frac{1}{4}W^a_{\mu\nu}W^{a\mu\nu} - \frac{1}{4}B_{\mu\nu}B^{\mu\nu}\\ &+ (D_\mu H)^\dagger (D^\mu H) + \mu^2 H^\dagger H - \lambda (H^\dagger H)^2\\ &+ \overline{L_i} i \not{D} L_i + \overline{e_{Ri}} i \not{D} e_{Ri}\\ &- Y^e_{ij}(\overline{L_i} e_{Rj} H + H^\dagger \overline{e_{Rj}} L_i)\end{aligned} \tag{1}$$

with the gauge-covariant derivative

$$D_\mu = \partial_\mu - i g_2 W^a_\mu T^a - i g_1 Y B_\mu,$$
$$T^a = \begin{cases} \dfrac{\sigma^a}{2} & \text{EW doublet} \\ 0 & \text{EW singlet} \end{cases}, \tag{2}$$

in terms of the Pauli matrices σ^a with $a = 1, 2, 3$.

2.1 Effective field theory

2.1.1 SMEFT

In the Standard Model Effective Field Theory (SMEFT) we extend the SM Lagrangian with a set of dimension-five and -six operators $\mathcal{O}_i$:

$$\mathcal{L} = \mathcal{L}_{\text{SM}} + \sum_i C_i \mathcal{O}_i. \tag{3}$$

In our convention the Wilson coefficients C_i are dimensional; for later use we also define the dimensionless variants $\hat{C}_i \equiv C_i \times \text{TeV}^2$ of the dimension-six coefficients.

The conventional basis of operators is the so-called *Warsaw basis* [73]. For the convenience of the reader, we reproduce the most relevant operators for the fermionic Seesaw models (additional operators relevant to Higgsstrahlung are also listed in Table 2):

$$\begin{aligned}\mathcal{L} \supset &\left[C_{5,ij}\,(\widetilde{H}^\dagger L_i)^T C (\widetilde{H}^\dagger L_j) + \text{h.c.}\right]\\ &+ \left[C_{eB,ij}\,(\overline{L_i}\sigma^{\mu\nu} e_{Rj}) H B_{\mu\nu} + \text{h.c.}\right]\\ &+ \left[C_{eW,ij}\,(\overline{L_i}\sigma^{\mu\nu}\sigma^a e_{Rj}) H W^a_{\mu\nu} + \text{h.c.}\right]\\ &+ \left[C_{eH,ij}\,(H^\dagger H)(\overline{L_i} e_{Rj} H) + \text{h.c.}\right]\\ &+ C^{(1)}_{HL,ij}\,(H^\dagger i \overleftrightarrow{D}_\mu H)(\overline{L_i}\gamma^\mu L_j)\\ &+ C^{(3)}_{HL,ij}\,(H^\dagger i \overleftrightarrow{D}^a_\mu H)(\overline{L_i}\sigma^a\gamma^\mu L_j),\end{aligned} \tag{4}$$

with $\widetilde{H} = i\sigma_2 H^*$, and C the charge conjugation matrix satisfying $C^\dagger\gamma^\mu C = -(\gamma^\mu)^T$.

In addition to directly contributing to physical processes, the SMEFT operators also modify the relations between observed quantities and SM parameters, as well as the relations between different parameters. The result of these effects is that the SM parameters will be numerically different in SMEFT compared to the SM. For example, the measured value of the Fermi constant, $\hat{G}_F$, in muon decay will differ from its standard expression $G_F = 1/(\sqrt{2}v_T^2)$, v_T being the Higgs VEV in SMEFT (see e.g. Ref. [74]), by

$$\delta\hat{G}_F = \hat{G}_F - G_F = \frac{1}{\sqrt{2}}\left(C^{(3)}_{HL,11} + C^{(3)}_{HL,22}\right) - \frac{1}{2\sqrt{2}}(C_{LL,1221} + C_{LL,2112}). \quad (5)$$

When computing the shift in a quantity such as a cross section from its SM value, one must therefore take care to include the contributions from these parameter shifts. Concretely, if $\sigma_{\rm SM}(g_i)$ is a cross section computed in the SM written as a function of the parameters g_i, then

$$\Delta\sigma = \sigma_{\rm SMEFT} - \sigma_{\rm SM} = \Delta\sigma_{\rm Direct} + \sum_i \frac{\partial\sigma_{\rm SM}}{\partial g_i}\delta g_i, \quad (6)$$

where $\Delta\sigma_{\rm Direct}$ captures direct contributions of new operators, and δg_i is the shift in the parameter g_i. The values of the parameter shifts critically depend on one's choice of input parameters; in this work we use (α, m_Z, G_F) as our electroweak inputs. A thorough review of such shifts may be found for instance in Ref. [75], and we provide additional exposition in Appendix A.

2.1.2 LEFT

To describe physics taking place at scales below the electroweak scale we utilise Low-Energy Effective Field Theory (LEFT). The relevant part of the Lagrangian for purely leptonic transitions reads in the Jenkins–Manohar–Stoffer (JMS) basis [76]

$$\begin{aligned}\mathcal{L} \supset\ & C^{VLL}_{ee,ijkl}(\overline{\ell_i}\gamma^\mu P_L \ell_j)(\overline{\ell_k}\gamma_\mu P_L \ell_l) \\ & + C^{VRR}_{ee,ijkl}(\overline{\ell_i}\gamma^\mu P_R \ell_j)(\overline{\ell_k}\gamma_\mu P_R \ell_l) \\ & + C^{VLR}_{ee,ijkl}(\overline{\ell_i}\gamma^\mu P_L \ell_j)(\overline{\ell_k}\gamma_\mu P_R \ell_l) \\ & + \left[C_{e\gamma,ij}(\overline{\ell_i}\sigma^{\mu\nu} P_R \ell_j)F_{\mu\nu} + \text{h.c.}\right]. \end{aligned} \quad (7)$$

We define the covariant derivative in QED as in $D_\mu = \partial_\mu + iQeA_\mu$, following Ref. [76]. For semi-leptonic neutral-current transitions, the relevant part of the Lagrangian is

$$\begin{aligned}\mathcal{L}\ \supset\ & C^{VLL}_{eq}(\overline{\ell}\gamma^\mu P_L \ell)(\overline{q}\gamma_\mu P_L q) \\ & + C^{VRR}_{eq}(\overline{\ell}\gamma^\mu P_R \ell)(\overline{q}\gamma_\mu P_R q) \\ & + C^{VLR}_{eq}(\overline{\ell}\gamma^\mu P_L \ell)(\overline{q}\gamma_\mu P_R q) \\ & + C^{VLR}_{qe}(\overline{q}\gamma^\mu P_L q)(\overline{\ell}\gamma_\mu P_R \ell). \end{aligned} \quad (8)$$

To obtain the LEFT Wilson coefficients for the Seesaw models introduced below, we utilise the software package `DsixTools` [77] to (i) compute the renormalisation group (RG) running of the SMEFT coefficients between the Seesaw scale and the electroweak scale, $\mu = m_Z$, (ii) match the SMEFT and LEFT coefficients, and (iii) run the LEFT coefficients to the low scale $\mu = 5\,\text{GeV}$. As there are no sizeable contributions to quark-field operators in the Seesaw models, we assume that this procedure captures the main contributions from RG running in LEFT, and further effects at lower scales do not appreciably change the results. See Appendix B for more details.

2.2 Seesaw models

2.2.1 Type-I

In the Type-I Seesaw model [43–47] the SM Lagrangian is extended by adding n_ν right-handed sterile neutrinos $\{\nu_{Ri}\}_{i=1}^{n_\nu}$ (so that there are a total of $3+n_\nu$ neutrinos), accompanied by a new Yukawa interaction to generate Dirac neutrino masses, as well as Majorana mass terms for the ν_R:

$$\begin{aligned}\mathcal{L}_{\nu_R} = & \sum_{i=1}^{n_\nu} \overline{\nu_{Ri}} i\not{\partial} \nu_{Ri} - \frac{1}{2}\sum_{i,j=1}^{n_\nu}\left(M^\nu_{ij}\overline{\nu^c_{Ri}}\nu_{Rj} + \text{h.c.}\right) \\ & - \sum_{i=1}^{3}\sum_{j=1}^{n_\nu}\left(Y^\nu_{ij}\overline{L_i}\nu_{Rj}\widetilde{H} + \text{h.c.}\right), \end{aligned} \quad (9)$$

where the conjugate fields ν^c are defined as $\nu^c \equiv \gamma^0 C\nu^*$ [81]. After electroweak symmetry breaking we are able to express the combined mass terms as the matrix equation

$$\mathcal{L}_{\nu\ \text{mass}} = -\frac{1}{2}\begin{pmatrix}\overline{\nu_L} & \overline{\nu^c_R}\end{pmatrix}\begin{pmatrix}0 & m^\nu \\ m^{\nu T} & M^\nu\end{pmatrix}\begin{pmatrix}\nu^c_L \\ \nu_R\end{pmatrix} + \text{h.c.}, \quad (10)$$

where we refer to $m^\nu_{ij} \equiv Y^\nu_{ij} v/\sqrt{2}$ as the Dirac mass matrix, and M^ν is the Majorana mass matrix. Matching this theory onto SMEFT at the scale $\mu = M^\nu$ yields the effective operators collected on the left side of Table 1.

2.2.2 Type-III

In the Type-III Seesaw model [48] the SM Lagrangian is extended by adding n_Σ right-handed weak fermion triplets $\{\Sigma^a_{Ri}\}_{i=1}^{n_\Sigma}$ with vanishing hypercharge, a new Yukawa interaction to generate Dirac neutrino masses, and Majorana mass terms for the Σ_R [69,82]:

$$\begin{aligned}\mathcal{L}_{\Sigma_R} = & \sum_{i=1}^{n_\Sigma}\overline{\Sigma_{Ri}} i\not{D}\Sigma_{Ri} - \frac{1}{2}\sum_{i,j=1}^{n_\Sigma}\left(M^\Sigma_{ij}\,\overline{\Sigma^c_{Ri}}\Sigma_{Rj} + \text{h.c.}\right) \\ & - \sum_{i=1}^{3}\sum_{j=1}^{n_\Sigma}\left(Y^\Sigma_{ij}\overline{L_i}\sigma^a\Sigma^a_{Rj}\widetilde{H} + \text{h.c.}\right), \end{aligned} \quad (11)$$

where $a = 1, 2, 3$ is elided from all but the Yukawa term. For a fixed triplet generation i, the eigenstates of electric charge are given by the combinations [69]

$$\Sigma^\pm_{Ri} \equiv \frac{\Sigma^1_{Ri} \mp i\Sigma^2_{Ri}}{\sqrt{2}}, \quad \Sigma^0_{Ri} \equiv \Sigma^3_{Ri}. \quad (12)$$

Table 1 SMEFT Wilson coefficients obtained from matching the Type-I and Type-III Seesaw models at the scale $\mu = M^X$ [78–80]. In order to properly account for the stringent bounds from the non-observation of lepton flavour violation, the electroweak dipole operators C_{eB} and C_{eW} (last two rows) are matched to one-loop order, while all other operators are matched at tree level

Coefficient	Type-I	Type-III
$C_{5,ij}$	$\frac{1}{2}\left(Y^{\nu *}(M^{\nu\dagger})^{-1}Y^{\nu\dagger}\right)_{ij}$	$\frac{1}{2}(Y^{\Sigma *}(M^{\Sigma\dagger})^{-1}Y^{\Sigma\dagger})_{ij}$
$C^{(1)}_{HL,ij}$	$\frac{1}{4}\left(Y^{\nu}(M^{\nu\dagger}M^{\nu})^{-1}Y^{\nu\dagger}\right)_{ij}$	$\frac{3}{4}\left(Y^{\Sigma}(M^{\Sigma\dagger}M^{\Sigma})^{-1}Y^{\Sigma\dagger}\right)_{ij}$
$C^{(3)}_{HL,ij}$	$-\frac{1}{4}\left(Y^{\nu}(M^{\nu\dagger}M^{\nu})^{-1}Y^{\nu\dagger}\right)_{ij}$	$\frac{1}{4}\left(Y^{\Sigma}(M^{\Sigma\dagger}M^{\Sigma})^{-1}Y^{\Sigma\dagger}\right)_{ij}$
$C_{eH,ij}$	0	$\left(Y^{\Sigma}(M^{\Sigma\dagger}M^{\Sigma})^{-1}Y^{\Sigma\dagger}Y^{e}\right)_{ij}$
$C_{eB,ij}$	$\frac{1}{16\pi^2}\frac{g_1}{24}\left(Y^{\nu}(M^{\nu\dagger}M^{\nu})^{-1}Y^{\nu\dagger}Y^{e}\right)_{ij}$	$\frac{1}{16\pi^2}\frac{g_1}{8}\left(Y^{\Sigma}(M^{\Sigma\dagger}M^{\Sigma})^{-1}Y^{\Sigma\dagger}Y^{e}\right)_{ij}$
$C_{eW,ij}$	$\frac{1}{16\pi^2}\frac{5g_2}{24}\left(Y^{\nu}(M^{\nu\dagger}M^{\nu})^{-1}Y^{\nu\dagger}Y^{e}\right)_{ij}$	$\frac{1}{16\pi^2}\frac{3g_2}{8}\left(Y^{\Sigma}(M^{\Sigma\dagger}M^{\Sigma})^{-1}Y^{\Sigma\dagger}Y^{e}\right)_{ij}$

In a manner completely analogous to the Type-I Seesaw model, after electroweak symmetry breaking we obtain the neutrino mass matrix

$$\mathcal{L}_{\nu\,\text{mass}} = -\frac{1}{2}\begin{pmatrix}\overline{\nu_L} & \overline{\Sigma^{0c}_R}\end{pmatrix}\begin{pmatrix}0 & m^{\Sigma}\\ m^{\Sigma T} & M^{\Sigma}\end{pmatrix}\begin{pmatrix}\nu^c_L\\ \Sigma^0_R\end{pmatrix} + \text{h.c.}, \tag{13}$$

where we refer to $m^{\Sigma}_{ij} \equiv Y^{\Sigma}_{ij}v/\sqrt{2}$ as the Dirac mass matrix, and M^{Σ} is the Majorana mass matrix. The states $\Sigma^{\pm}_{Ri}$ instead mix into the charged leptons. Matching this theory onto SMEFT at the scale $\mu = M^{\Sigma}$ yields the effective operators collected on the right side of Table 1.

2.3 Conserved lepton-number symmetry

In this work, we study symmetry-protected versions of the fermionic Seesaw models, wherein a lepton-number (LN) symmetry decouples the physics of neutrino masses from the phenomenology associated with the conservation of LN [59,69–72]. Without loss of generality, we fix $n_\nu = n_\Sigma = 2$, that is, we focus on the case of two heavy fermion singlet or triplet interaction states which is consistent with at least two massive active neutrinos, as is dictated by neutrino oscillation data. The heavy fermion states are assigned 1 and -1 unit of LN, respectively. After electroweak symmetry breaking, the Dirac mass matrix is given by

$$m^X_{ij} = \frac{v}{\sqrt{2}}\left(Y^X\ \epsilon Y^{X'}\right)_{ij} = \frac{v}{\sqrt{2}}\begin{pmatrix}Y^{X_e} & \epsilon Y^{X'_e}\\ Y^{X_\mu} & \epsilon Y^{X'_\mu}\\ Y^{X_\tau} & \epsilon Y^{X'_\tau}\end{pmatrix}_{ij}, \tag{14}$$

and the Majorana mass matrix reads

$$M^X_{ij} = \begin{pmatrix}\mu_1 M^X & M^X\\ M^X & \mu_2 M^X\end{pmatrix}_{ij}, \tag{15}$$

where ϵ and $\mu_{1,2}$ are dimensionless parameters. We parametrise the mixing of the SM neutrino ν_i with the fermion singlet ν_{Ri}, or the neutral component Σ^0_{Ri} of the fermion triplet in terms of the dimensionless ratios

$$\theta_i = \frac{m^X_{i1}}{M^X} = \frac{Y^{X_i}}{\sqrt{2}}\frac{v}{M^X}, \tag{16}$$

which are equal to the active-sterile *mixing angles* in the small-mixing approximation, that is, if $\mathcal{O}\big((v/M^X)^3\big)$ effects are neglected. For simplicity, we will refer to θ_e also as the "electron(-flavour) mixing angle", and to $|\theta_e|$ as "electron(-flavour) mixing", and equivalently for the other flavours. Light neutrino masses are then proportional to ϵ and μ_2 which break LN:

$$m_\nu = \frac{v^2}{2}\Big[\mu_2 Y^X (M^X)^{-1} Y^{X^T} - \epsilon\left(Y^{X'}(M^X)^{-1}Y^{X^T} + Y^X(M^X)^{-1}Y^{X'^T}\right)\Big]. \tag{17}$$

The limit $\mu_2 \neq 0$ and $\mu_1 = \epsilon = 0$ is referred to as *inverse Seesaw* [62,83,84], and $\epsilon \neq 0$ and $\mu_{1,2} = 0$ is commonly known as *linear Seesaw* [85,86].[1]

We adopt the LN-conserving limit $\epsilon = \mu_{1,2} = 0$ with non-zero M^X in this work, which results in massless active neutrinos and a heavy Dirac neutrino of mass M^X, and hence assume the textures

$$Y^X_{ij} = \begin{pmatrix}Y^{X_e} & 0\\ Y^{X_\mu} & 0\\ Y^{X_\tau} & 0\end{pmatrix} \quad \text{and} \quad M^X_{ij} = \begin{pmatrix}0 & M^X\\ M^X & 0\end{pmatrix} \tag{18}$$

for both $X = \nu$ and Σ. In this way, we neglect the phenomenological implications of LN violation, and instead

[1] Note that with the help of Table 1 one can check that – as long as the contributions of the Weinberg operator to the dimension-six operators via RG running can be neglected – the only change resulting from $\mu_{1,2} \neq 0$ compared to the LN-conserving limit is $\theta_i^2 \to \frac{1+\mu_2^2}{(1+\mu_1\mu_2)^2}\theta_i^2$ for each mixing angle in all of our formulae.

focus on LN-conserving effects.[2] Note that one may add a further singlet or triplet with vanishing LN such that

$$Y^X_{ij} = \begin{pmatrix} Y^{X_e} & 0 & 0 \\ Y^{X_\mu} & 0 & 0 \\ Y^{X_\tau} & 0 & 0 \end{pmatrix} \quad \text{and}$$
$$M^X_{ij} = \begin{pmatrix} 0 & M^X & 0 \\ M^X & 0 & 0 \\ 0 & 0 & M^{X'} \end{pmatrix}, \tag{19}$$

which supports three massive active neutrinos if one departs from the LN-conserving limit. Still, the additional state trivially decouples from the phenomenology.[3]

3 Phenomenology

We choose the benchmark value $M^X = 1$ TeV for the masses of the new interaction states in our analysis. To our knowledge, this is consistent with all performed direct searches for heavy neutral leptons at colliders, see for instance Ref. [37] for a recent overview. In Ref. [88], for sterile neutrinos of a mass $M^\nu \approx 1$ TeV the constraint $|\theta_e| \sim |\theta_\mu| \lesssim \mathcal{O}(1)$ was derived via a search for the signature of three charged leptons with any combination of electron and muon flavours. Reference [89] reports the constraint $|\theta_\mu|^2 \lesssim \mathcal{O}(0.1)$ for TeV-scale Majorana neutrinos, based on a search for same-sign dimuon final states, see also Ref. [61]. The bound $M^{\Sigma_0} \geq 910$ GeV was derived in a recent study [90] which focuses on leptonic final states and takes into account earlier ATLAS results.

In our phenomenological discussion we consider the following observables:

- the relative shift $\Delta\sigma/\sigma_0$ in the Higgsstrahlung cross section from its SM prediction,
- the effective leptonic weak mixing angle $\sin^2(\theta^{\text{lept}}_{w,\text{eff}})$ and the W-boson mass m_W,
- the ratios $g^X_{\mu/e}$ and $g^X_{\tau/\mu}$ of leptonic gauge couplings as probes of lepton flavour universality (LFU), and the ratios $R(K_{\ell 3})$ and $R(V_{us})$, and
- the branching ratios of the LFV processes $\mu \to e\gamma$, $\mu \to 3e$, $\tau \to e\gamma$, $\tau \to 3e$, and the ratios of the $\mu - e$ conversion rates over the muon capture rate in different target nuclei.

In Tables 4, 5, 6 and 7, the theoretical expressions for these observables in the fermionic Seesaw models are listed as functions of the mixing angles θ_e, θ_μ, θ_τ, as defined in Eq. (16), for a matching scale $\mu = M^X = 1$ TeV. While our expressions hold for complex Yukawa couplings, we do not consider CP violation in the analysis and treat the mixings as real numbers which are only constrained from existing bounds on LN-conserving processes. If effects from RG running in SMEFT above the matching scale are neglected, one may naïvely interpret the results also for a larger mass and appropriately rescale the couplings. Nonetheless, we also computed the relevant expressions for $\mu = M^X = 10$ TeV, which is commented on in Sect. 3.5.

The following discussions are supported by plots in the θ_e–θ_μ plane, as well as plots in the θ_e–θ_τ plane for the LFU and LFV observables.[4] The third mixing angle is fixed to the benchmark values $\theta_\tau = 10^{-2}$ and $\theta_\mu = 10^{-6}$; these choices are most transparently justified (at least for Type-III) by Fig. 6, which depicts the most competitive constraints for both models. We have explicitly checked that there are no appreciable changes in the resulting phenomenology if these values are tuned smaller or even zero, apart from the fact that the LFV bounds become weaker and eventually vanish. In each of these plots we produce exclusion regions which either reflect the current bounds at 2σ for the electroweak and LFU observables, or the upper limits on the LFV processes at 90% C.L.

3.1 Higgsstrahlung

3.1.1 SM tree-level contribution

The tree-level differential cross section in the SM is well-known, and is given by [91,92]

$$\frac{\mathrm{d}\sigma_0}{\mathrm{d}\cos\theta} = \frac{\sqrt{\lambda}}{32\pi s^2}\overline{|\mathcal{M}_t{}^2|}, \tag{20}$$

where unpolarised beams are assumed, with

$$\overline{|\mathcal{M}_t|^2} = \frac{s}{2}(g_L^2 + g_R^2)\left(\frac{g_{ZZh}}{s - m_Z^2}\right)^2\left(1 + \frac{\lambda \sin^2\theta}{8sm_Z^2}\right) \tag{21}$$

[2] Note that this also means that the parameters θ_i can be treated as independent. If data on lepton mixing and the hierarchy of neutrino masses is to be properly accommodated, the θ_i exhibit non-trivial correlations as is discussed for instance in Refs. [82,87].

[3] As is discussed in Ref. [69], the determinant of the full neutrino mass matrix also vanishes in the (LN-violating) case $\mu_1 \neq 0$ and $\epsilon = \mu_2 = 0$, which however generally guarantees only one massless active neutrino. One may also consider a vanishing Majorana mass matrix and a completely general Dirac mass matrix instead of the textures assumed herein; nonetheless, this scenario yields light Dirac neutrinos and is not suitable for a study in SMEFT.

[4] We do not include plots in the θ_μ–θ_τ plane, as the major objective of our work is to investigate how the sensitivity of the fermionic Seesaw models to the Higgsstrahlung process compares to other observables, and we are thus primarily concerned with phenomenological effects related to electron flavour.

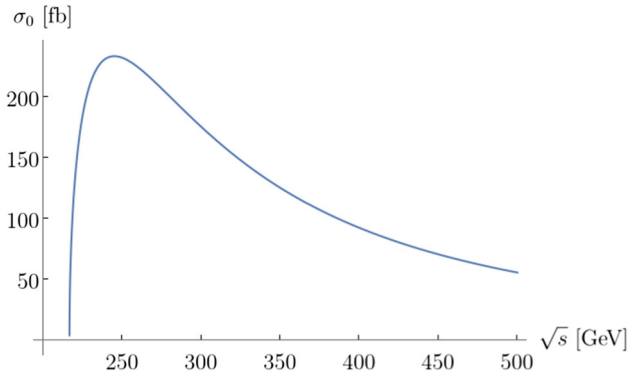

Fig. 1 The tree-level cross section for the Higgsstrahlung process in the SM as a function of the centre-of-mass energy $\sqrt{s}$

the spin-averaged matrix element. Here the couplings are

$$g_{ZZh} = \frac{g_2 m_Z}{\cos\theta_w}, \qquad g_L = g_Z(-\tfrac{1}{2} + \sin^2\theta_w),$$
$$g_R = g_Z \sin^2\theta_w, \qquad g_Z = \frac{g_2}{\cos\theta_w}, \tag{22}$$

θ is the angle between the incoming electron and outgoing Z boson, and

$$\lambda = (s - m_Z^2 - m_h^2)^2 - 4m_Z^2 m_h^2 \tag{23}$$

is the relevant Källèn function. The corresponding integrated cross section is

$$\sigma_0 = \frac{\sqrt{\lambda}}{32\pi s}(g_L^2 + g_R^2)\left(\frac{g_{ZZh}}{s - m_Z^2}\right)^2\left(1 + \frac{\lambda}{12 s m_Z^2}\right). \tag{24}$$

The dependence of σ_0 on $\sqrt{s}$ is depicted in Fig. 1. It peaks around a centre-of-mass energy of $\sqrt{s} \approx 245\,\text{GeV}$.

3.1.2 Corrections in SMEFT

Including corrections from new physics, we write

$$\frac{\mathrm{d}\sigma}{\mathrm{d}\cos\theta} = \frac{\sqrt{\lambda}}{32\pi s^2}\left(\overline{|\mathcal{M}_t|^2} + \delta\overline{|\mathcal{M}_t|^2} + 2\Re\overline{\mathcal{M}_t^* \mathcal{M}_c}\right), \tag{25}$$

where $\delta\overline{|\mathcal{M}_t|^2}$ denotes the effect of parameter shifts in SMEFT to the tree-level cross section, as discussed in Sect. 2.1.1, and $2\Re\overline{\mathcal{M}_t^* \mathcal{M}_c}$ is the interference term of the tree-level amplitude with corrections from new operators. The explicit result reads[5]

$$\Delta\frac{\mathrm{d}\sigma}{\mathrm{d}\cos\theta} = \frac{\sqrt{\lambda}}{32\pi s^2}\left[2\left(\frac{\delta g_{ZZh}}{g_{ZZh}} + \frac{g_L\delta g_L + g_R\delta g_R}{g_L^2 + g_R^2}\right)\overline{|\mathcal{M}_t|^2} + \frac{g_{ZZh} v}{2}\sum_{i=2}^{5} d_i F_i\right], \tag{26}$$

where the parameter shifts and coefficients d_i are presented below, and the form factors F_i may be found in Ref. [92].

The full resulting fractional shift for the cross section is

$$\frac{\Delta\sigma}{\sigma_0} = 2\left(\frac{\delta g_{ZZh}}{g_{ZZh}} + \frac{g_L\delta g_L + g_R\delta g_R}{g_L^2 + g_R^2}\right) + \frac{v}{g_{ZZh}}\sum_{i=2}^{5} d_i f_i. \tag{27}$$

Here the parameter shifts in the (α, m_Z, G_F) input scheme are

$$\begin{aligned}
\frac{\delta g_{ZZh}}{g_{ZZh}} &= v_T^2\left(C_{H\Box} + \frac{1}{4}C_{HD} - \frac{1}{\sqrt{2}}\delta\hat{G}_F\right),\\
\frac{\delta g_L}{g_Z} &= \frac{1}{8(c_w^2 - s_w^2)}v_T^2\Big(8 s_w c_w C_{HWB} + C_{HD} + 2\sqrt{2}\,\delta\hat{G}_F\Big) - \frac{1}{2}v_T^2\left(C_{HL,11}^{(1)} + C_{HL,11}^{(3)}\right),\\
\frac{\delta g_R}{g_Z} &= \frac{s_w^2}{4(c_w^2 - s_w^2)}v_T^2\Big(4\frac{c_w}{s_w}C_{HWB} + C_{HD} + 2\sqrt{2}\,\delta\hat{G}_F\Big) - \frac{1}{2}v_T^2 C_{He,11},
\end{aligned} \tag{28}$$

where we adopt the shorthands $s_w \equiv \sin\theta_w$ and $c_w \equiv \cos\theta_w$, and $\delta\hat{G}_F$ is defined in Eq. (5). The integrated form factors f_i are

$$f_2 = 12 m_Z^2 \frac{s(s + m_Z^2 - m_h^2)}{12 s m_Z^2 + \lambda}, \tag{29a}$$

$$f_3 = -12 e m_Z^2 \frac{g_L + g_R}{g_L^2 + g_R^2}\frac{(s - m_Z^2)(s + m_Z^2 - m_h^2)}{12 s m_Z^2 + \lambda}, \tag{29b}$$

$$f_4 = \frac{2 g_L}{g_L^2 + g_R^2}(s - m_Z^2), \quad \text{and} \tag{29c}$$

$$f_5 = \frac{2 g_R}{g_L^2 + g_R^2}(s - m_Z^2), \tag{29d}$$

and their corresponding coefficients d_i are

$$d_2 = 4(s_w^2 C_{HB} + s_w c_w C_{HWB} + c_w^2 C_{HW}), \tag{30a}$$

$$d_3 = -4 s_w c_w C_{HB} - 2(c_w^2 - s_w^2)C_{HWB} + 4 s_w c_w C_{HW}, \tag{30b}$$

$$d_4 = -g_Z(C_{HL,11}^{(1)} + C_{HL,11}^{(3)}), \quad \text{and} \tag{30c}$$

$$d_5 = -g_Z C_{He,11}. \tag{30d}$$

[5] See Ref. [91] for a calculation of the Higgsstrahlung cross section in the Type-I Seesaw model which does not rely on effective field theory.

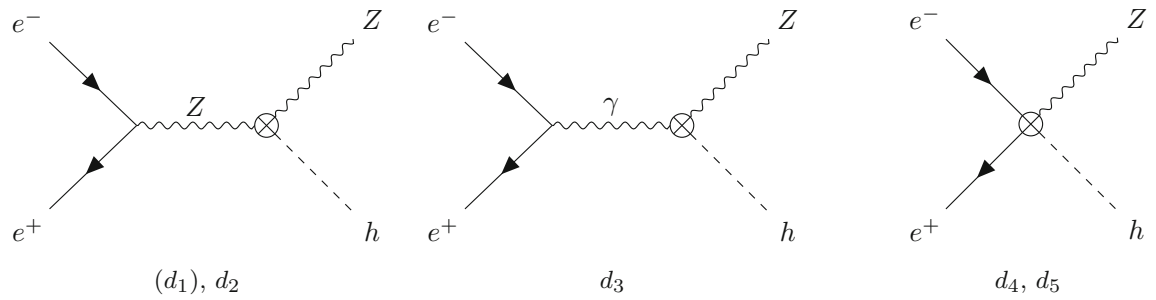

Fig. 2 Diagrams with effective vertices contributing to Eq. (27)

Table 2 Dimension-6 SMEFT operators in the Warsaw basis [73] which enter the correction to the Higgsstrahlung cross section. Here $H^\dagger i\overleftrightarrow{D}^a_\mu H \equiv i H^\dagger \sigma^a D_\mu H - i(D_\mu H)^\dagger \sigma^a H$

$\mathcal{O}_{HW}$	$H^\dagger H W^a_{\mu\nu} W^{a\mu\nu}$
$\mathcal{O}_{HB}$	$H^\dagger H B_{\mu\nu} B^{\mu\nu}$
$\mathcal{O}_{HWB}$	$H^\dagger \sigma^a H W^a_{\mu\nu} B^{\mu\nu}$
$\mathcal{O}_{H\Box}$	$(H^\dagger H)\Box(H^\dagger H)$
$\mathcal{O}_{HD}$	$(H^\dagger D_\mu H)^*(H^\dagger D^\mu H)$
$\mathcal{O}_{LL,ijkl}$	$(\overline{L_i}\gamma^\mu L_j)(\overline{L_k}\gamma_\mu L_l)$
$\mathcal{O}^{(1)}_{HL,ij}$	$(H^\dagger i\overleftrightarrow{D}_\mu H)(\overline{L_i}\gamma^\mu L_j)$
$\mathcal{O}^{(3)}_{HL,ij}$	$(H^\dagger i\overleftrightarrow{D}^a_\mu H)(\overline{L_i}\sigma^a\gamma^\mu L_j)$
$\mathcal{O}_{He,ij}$	$(H^\dagger i\overleftrightarrow{D}^a_\mu H)(\overline{e_{Ri}}\gamma^\mu e_{Rj})$

The diagrams giving rise to the d_i's are depicted in Fig. 2. Note that d_1 and f_1 are absent here, as we have elected instead to absorb their contribution into δg_{ZZh}. The dimension-six SMEFT operators which constitute these corrections are listed in Table 2. We comment that the d_i's are zero at tree level in the Seesaw models, apart from d_4 in Type-III.

3.1.3 Discussion

An essential part of the program of most of the proposed next-generation lepton colliders is to be run as "Higgs factories" at a centre-of-mass energy of $\sqrt{s} = 240\,\text{GeV}$ (CEPC, FCC-ee) or 250 GeV (ILC), and to perform a scan of the $t\bar{t}$ production threshold in the range $\sqrt{s} = 350$–$380\,\text{GeV}$. Measurements of the Higgsstrahlung cross section are foreseen at both stages for all collider proposals considered herein, apart from CLIC which is envisioned to directly run at $\sqrt{s} = 380\,\text{GeV}$ in its initial stage. Therefore, we evaluate the relative shift $\Delta\sigma/\sigma_0$ of the Higgsstrahlung cross section, computed in Eq. (27), at $\sqrt{s} = 240\,\text{GeV}$ and 365 GeV. Regarding the precision of the measurement, we assume the two benchmark values of 0.5% and 1.0% for $\sqrt{s} = 240\,\text{GeV}$, and 1.0% for $\sqrt{s} = 365\,\text{GeV}$. This is representative of the results of several conducted studies of the attainable precision, which are collected in Table 3.

The shifts in the cross section as functions of the mixing angles are listed for both Seesaw models in Table 4. To aid in the following discussion, we moreover find for $\sqrt{s} = 240\,\text{GeV}$

$$\frac{\Delta\sigma}{\sigma_0} \approx 0.90\,\hat{C}^{(1)}_{HL,11} + 0.77\,\hat{C}^{(3)}_{HL,11} - 0.13\,\hat{C}^{(3)}_{HL,22}, \tag{31}$$

and for $\sqrt{s} = 365\,\text{GeV}$

$$\frac{\Delta\sigma}{\sigma_0} \approx 2.09\,\hat{C}^{(1)}_{HL,11} + 1.96\,\hat{C}^{(3)}_{HL,11} - 0.13\,\hat{C}^{(3)}_{HL,22}, \tag{32}$$

where the Wilson coefficients are evaluated at $\mu = \sqrt{s}$, respectively, and as a reminder, we define the dimensionless Wilson coefficients by $\hat{C} = C \times \text{TeV}^2$. These approximate expressions deviate from the exact results, presented in Table 4, by maximally 5% in either model.

As the couplings of the Z boson to charged leptons are not directly altered at tree level in the Type-I Seesaw model, $\sigma(e^+e^- \to Zh)$ is predominantly modified via the shift in the Fermi constant, Eq. (5), which enters through the shifts δg_{ZZh}, δg_L, and δg_R in Eq. (28). While the contributions of electron and muon mixing are of fairly similar magnitudes, $\Delta\sigma/\sigma_0$ turns out to be slightly more sensitive to the latter. This is due to a partial cancellation of the coefficient d_4 in Eq. (30c) (which acquires a nonzero value from RG running) against the dominant contribution from the Fermi constant for electron mixing. As the corresponding form factor f_4 scales with s, the resulting sensitivity to electron mixing shrinks even further at higher energies. Consequently, if sterile neutrinos are to be searched for via precision Higgs measurements, we do not expect running a next-generation lepton collider at higher centre-of-mass energies to reveal much for Type-I.

Contrariwise, in Type-III the couplings of the Z boson to left-handed charged leptons are modified at tree level which results in a sizeable contribution to d_4. That is, in an EFT language, the model induces the effective four-point interaction $\bar{e}\gamma^\mu P_L e Z_\mu h$ depicted on the right in Fig. 2 which interferes with the tree-level contribution to Higgsstrahlung in the SM.

Table 3 Forecast (statistical) precision of measurements of the Higgsstrahlung cross section at different proposed next-generation colliders. In the third column, the Z-decay final states taken into account in the respective analysis are given; $\ell^+\ell^-$ always implies both $Z \to e^+e^-$ and $Z \to \mu^+\mu^-$. For the results from Ref. [93] a polarisation $(P_{e^-}, P_{e^+}) = (-80\%, +30\%)$ is assumed, still, this changes the expected Higgsstrahlung event rate by maximally 50% compared to unpolarised beams [58,94]. No polarisation is assumed for the ILC precision for $\sqrt{s} = 350\,\text{GeV}$ and hadronic Z-boson decays in Ref. [94], wherein an attainable precision of 1.76% for polarised beams and an integrated luminosity of $0.35\,\text{ab}^{-1}$ is reported as well

Collider	$L_{\text{int}}\,[\text{ab}^{-1}]$	Z-decay final states	$\sqrt{s}\,[\text{GeV}]$	Precision
CEPC	20	$\ell^+\ell^-, q\bar{q}, \nu\bar{\nu}$	240	0.26% [6]
	1	$\ell^+\ell^-, q\bar{q}, \nu\bar{\nu}$	360	1.4% [6]
FCC-ee	5	$\ell^+\ell^-$	240	0.5% [14]
	1.5	$\ell^+\ell^-, q\bar{q}, \nu\bar{\nu}$	365	0.9% [14]
ILC	1.35	$\ell^+\ell^-$	250	1.1% [93]
	0.115 (0.5)	$\ell^+\ell^-$ $(q\bar{q})$	350	5% (1.63%) [93,94]
	1.6 (0.5)	$\ell^+\ell^-$ $(q\bar{q})$	500	2.9% (3.9%) [93,95]
CLIC	0.5	$\ell^+\ell^-, q\bar{q}$	350	1.65% [58]

Table 4 Shifts of the Higgsstrahlung cross section at different centre-of-mass energies in terms of the mixing angles, when $M^X = 1\,\text{TeV}$. For the sake of comparison, we have also computed them for the larger centre-of-mass energy $\sqrt{s} = 500\,\text{GeV}$

	Type-I	Type-III
$\Delta\sigma/\sigma_0$ (240 GeV)	$0.95\,\lvert\theta_e\rvert^2 + 1.10\,\lvert\theta_\mu\rvert^2 + 0.02\,\lvert\theta_\tau\rvert^2$	$27.59\,\lvert\theta_e\rvert^2 - 1.08\,\lvert\theta_\mu\rvert^2 - 0.01\,\lvert\theta_\tau\rvert^2$
$\Delta\sigma/\sigma_0$ (365 GeV)	$0.87\,\lvert\theta_e\rvert^2 + 1.12\,\lvert\theta_\mu\rvert^2 + 0.04\,\lvert\theta_\tau\rvert^2$	$66.15\,\lvert\theta_e\rvert^2 - 1.09\,\lvert\theta_\mu\rvert^2 - 0.01\,\lvert\theta_\tau\rvert^2$
$\Delta\sigma/\sigma_0$ (500 GeV)	$0.80\,\lvert\theta_e\rvert^2 + 1.14\,\lvert\theta_\mu\rvert^2 + 0.05\,\lvert\theta_\tau\rvert^2$	$126.39\,\lvert\theta_e\rvert^2 - 1.10\,\lvert\theta_\mu\rvert^2 - 0.01\,\lvert\theta_\tau\rvert^2$

As the latter is suppressed by s due to the Z-boson propagator, this results in a very pronounced sensitivity of the ratio $\Delta\sigma/\sigma_0$ to electron mixing which approximately scales with s. Consequently, if enough luminosity can be attained to compensate for smaller statistics, fermion triplets may well be searched for in Higgsstrahlung measurements at larger centre-of-mass energies. Note that the contributions from electron mixing could in principle be (partly) cancelled by large muon mixing, however, we will find that this scenario is tightly constrained by existing phenomenological bounds. From Table 4 one can immediately deduce that if only electron mixing is sizeable, a minimal shift of $\Delta\sigma/\sigma_0 \geq 1\%$ for $\sqrt{s} = 240\,\text{GeV}$ requires $|\theta_e| \gtrsim 0.019$, whereas $|\theta_e| \gtrsim 0.013$ is sufficient if the relative cross-section shift can be as small as 0.5%, or if $\sqrt{s} = 365\,\text{GeV}$ is considered instead.

3.2 Electroweak sector

In this section, we introduce the shifts in the weak mixing angle and the mass of the W boson. The expressions obtained for the fermionic Seesaw models in terms of the mixing angles are listed in Table 5.

3.2.1 Weak mixing angle

In SMEFT the weak mixing angle is modified in accordance with (see e.g. Ref. [74])

$$\delta s_w^2 = \frac{c_w s_w}{c_w^2 - s_w^2} v_T^2 \left(\frac{1}{2} c_w s_w C_{HD} + C_{HWB} + \sqrt{2} c_w s_w\, \delta\hat{G}_F \right), \tag{33}$$

where the shift in the Fermi constant $\delta\hat{G}_F$ is defined in Eq. (5). There are numerous ways to extract the weak mixing angle from data; the most precise determination is that of the *effective leptonic weak mixing angle* $s^2_{w,\text{eff}} \equiv \sin^2(\theta^{\text{lept}}_{w,\text{eff}})$ at LEP [97], achieved via measurements of the left-right asymmetry factor

$$\mathcal{A}_f = \frac{g_L^2 - g_R^2}{g_L^2 + g_R^2} = \frac{2(1 - 4s_w^2)}{1 + (1 - 4s_w^2)^2}. \tag{34}$$

Apart from the general shift in Eq. (33), we must also take into account the fact that a modification of the Z couplings to charged leptons will directly affect the extraction of $s^2_{w,\text{eff}}$ from $\mathcal{A}_f$. Incorporating the "direct" shifts to these couplings,

$$\delta g^{\text{direct}}_{L,ij} = -\frac{1}{2} g_Z v_T^2 \left(C^{(1)}_{HL,ij} + C^{(3)}_{HL,ij} \right) \quad \text{and}$$
$$\delta g^{\text{direct}}_{R,ij} = -\frac{1}{2} g_Z v_T^2 C_{He,ij}, \tag{35}$$

we find

$$s^2_{w,\text{eff}} = s^2_{w,\text{SM}} + \delta s_w^2$$

Table 5 SM predictions for and current measurements of the electroweak observables considered in this work, together with approximate expressions for their shifts in terms of the mixing angles. The W-boson mass listed in the PDG [98] corresponds to the mass parameter in a Breit–Wigner distribution with a mass-dependent width. The SM prediction for the effective leptonic weak mixing angle is taken from Table II in Ref. [96]. The model predictions are obtained from matching onto SMEFT at the Seesaw scale $\mu = M^X = 1\,\text{TeV}$ and running to the electroweak scale $\mu = m_Z$

Electroweak sector		
Observable	SM prediction	Measurement
$\sin^2(\theta_{\text{eff}}^{\text{lept}})$	0.231534 ± 0.000030 [96]	0.23153 ± 0.00026 [97]
m_W [GeV]	80.356 ± 0.006 [98]	80.377 ± 0.012 [98]
Shift	Type-I	Type-III
δs_w^2	$-0.157(\lvert\theta_e\rvert^2 + \lvert\theta_\mu\rvert^2) + 0.003\,\lvert\theta_\tau\rvert^2$	$0.017(\lvert\theta_e\rvert^2 + \lvert\theta_\mu\rvert^2) - 0.143\,\lvert\theta_\tau\rvert^2$
$\delta m_W/\text{GeV}$	$8.24(\lvert\theta_e\rvert^2 + \lvert\theta_\mu\rvert^2) - 0.13\,\lvert\theta_\tau\rvert^2$	$-8.51(\lvert\theta_e\rvert^2 + \lvert\theta_\mu\rvert^2) - 0.13\,\lvert\theta_\tau\rvert^2$

$$
\begin{aligned}
&+ \frac{1}{3}\frac{\mathrm{d}s_w^2}{\mathrm{d}\mathcal{A}_\ell}\left(\frac{\partial \mathcal{A}_\ell}{\partial g_L}\sum_{i=1}^{3}\delta g_{L,ii}^{\text{direct}} + \frac{\partial \mathcal{A}_\ell}{\partial g_R}\sum_{i=1}^{3}\delta g_{R,ii}^{\text{direct}}\right)\\
&\approx s^2_{w,\text{SM}} + 0.020\left(\hat{C}^{(3)}_{HL,11} + \hat{C}^{(3)}_{HL,22}\right)\\
&\quad - 0.005\sum_{i=1}^{3}\left(\hat{C}^{(1)}_{HL,ii} + \hat{C}^{(3)}_{HL,ii}\right), \qquad (36)
\end{aligned}
$$

where the right-hand side is evaluated at the scale $\mu = m_Z$. Contributions from C_{He} are not sourced at tree level in either fermionic Seesaw model and thus we neglect them in the approximate expression above.

3.2.2 *W-boson mass*

The shift incurred in SMEFT is [74]

$$
\begin{aligned}
\frac{\delta m_W^2}{m_W^2} = &-\frac{1}{2(c_w^2 - s_w^2)}v_T^2\Big(4c_w s_w C_{HWB}\\
&+c_w^2 C_{HD} + 2\sqrt{2}s_w^2\,\delta\hat{G}_F\Big), \qquad (37)
\end{aligned}
$$

which approximately evaluates to

$$
m_W \approx m_{W,\text{SM}} - 1.05\left(\hat{C}^{(3)}_{HL,11} + \hat{C}^{(3)}_{HL,22}\right)\,\text{GeV} \qquad (38)
$$

at the scale $\mu = m_Z$. Evidently, the predicted W-boson mass is mainly sensitive to $\mathcal{O}^{(3)}_{HL}$ as the major correction is induced via the modified extraction of the Fermi constant in the fermionic Seesaw models.

3.2.3 *Discussion*

The constraints arising from the electroweak observables $s^2_{w,\text{eff}}$ and m_W are illustrated in Fig. 3.

For Type-I Seesaw one immediately notices that observing a deviation in the Higgsstrahlung cross section is already in direct conflict with the determination of $s^2_{w,\text{eff}}$, with a 0.5% shift at $\sqrt{s} = 240\,\text{GeV}$ suffering from a 2.9σ tension, and a 1% shift excluded at $\sim 6\sigma$. While this tension can be reduced by turning up θ_τ (see the expression in Table 5), LFU constraints discussed in Sect. 3.3 below preclude this from occurring. Thus, the Type-I Seesaw model is unlikely to be a viable minimal SM extension that can be probed in precision Higgs measurements, unless a significant reduction of the statistical uncertainty of these measurements can be attained.

In the Type-III Seesaw model, the effects of the triplets contributing to the extraction of the Fermi constant and from direct contributions to the leptonic gauge couplings largely cancel out, which equally applies to electron and muon flavour, see Eq. (36). Thus, $s^2_{w,\text{eff}}$ acts as a rather weak constraint on the Type-III Seesaw model, and is in fact most relevant for tau-flavour mixing, implying $|\theta_\tau| \lesssim 0.06$ at 2σ.

The existing tension between the SM prediction for the W-boson mass m_W and the larger experimental world average is however exacerbated in Type-III, leading to a much stronger constraint. In contrast, as $C^{(3)}_{HL}$ is induced with equal magnitude, but opposite signs via matching at the Seesaw scale in the two models under consideration, the tension can be alleviated in Type-I; if uncertainties are ignored, the current world average is reproduced for $\sqrt{|\theta_e|^2 + |\theta_\mu|^2} \approx 0.051$, and the CDF measurement [99] for $\sqrt{|\theta_e|^2 + |\theta_\mu|^2} \approx 0.097$. A detectable shift in $\sigma(e^+e^- \to Zh)$ could in principle only be induced in the latter case.

Testing the Type-III Seesaw model via Higgsstrahlung measurements is generally compatible with the current constraint arising from m_W. Still, it disfavours detectable $\Delta\sigma/\sigma_0$ induced via muon mixing, and clearly prefers contributions from electron mixing. The bound from m_W can be expected to become more competitive when the CDF measurement will be included in the experimental average in the future.

3.3 Lepton flavour universality

In SMEFT the $W\ell\nu$ coupling is directly altered due to $\mathcal{O}^{(3)}_{HL}$:

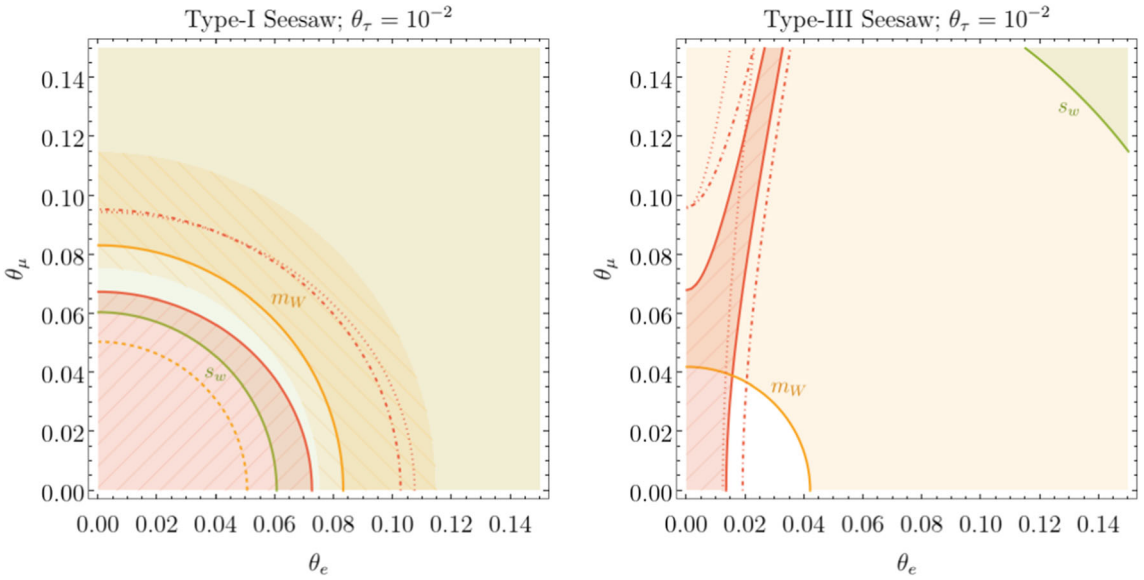

Fig. 3 Current constraints from electroweak observables at 2σ, in comparison with projected sensitivities of precision Higgsstrahlung measurements. The red-ruled regions indicate $|\Delta\sigma/\sigma| < 0.5\%$ at $\sqrt{s} = 240\,\text{GeV}$. The dot-dashed and dotted red lines are the corresponding 1% contours at $\sqrt{s} = 240\,\text{GeV}$ and $365\,\text{GeV}$, respectively. The ivory regions for large $\theta_{e,\mu}$ in the upper-right of the plots are excluded by measurements of both s_w and m_W. For Type-I Seesaw, the orange dashed line marks where the current experimental world average for m_W is exactly accommodated, and in the orange-ruled region the CDF measurement [99] is explained at 2σ

$$\mathcal{L} \supset -i\frac{g_2}{\sqrt{2}}\left(\delta_{ij} + v_T^2 C^{(3)}_{HL,ij}\right)\overline{\ell_i}\gamma^\mu P_L \nu_j W_\mu. \tag{39}$$

This modifies (semi-)leptonic decays mediated by W bosons, which, among other effects, drives the predictions for LFU ratios away from 1. In the following we consider ratios constituted by the leptonic decays $\pi \to \ell\nu$, $K \to \ell\nu$ and $\tau \to \ell\nu\bar{\nu}$. Furthermore, we utilise the extraction of the Cabibbo–Kobayashi–Maskawa (CKM)-matrix element V_{us} from the semi-leptonic decay $K_{\ell 3} : K \to \pi\ell\nu$ and from nuclear beta decays, together with the assumption of unitarity of the CKM matrix.

3.3.1 Ratios of leptonic gauge couplings

We consider the ratios of leptonic gauge couplings collected in Table 6 which are probes of LFU. For the first three listed therein, [102,103]

$$\begin{aligned} g^X_{\mu/e} \equiv \left(\frac{g_\mu}{g_e}\right)^X &\approx 1 + v_T^2 C^{(3)}_{HL,22} - v_T^2 C^{(3)}_{HL,11} \\ &\approx 1 + 0.06\left(\hat{C}^{(3)}_{HL,22} - \hat{C}^{(3)}_{HL,11}\right), \end{aligned} \tag{40}$$

where $(g_\mu/g_e)^X$ is the ratio of leptonic gauge couplings extracted from the ratio $\Gamma(X \to \mu\nu)/\Gamma(X \to e\nu)$ for $X = \pi, K$, and $\Gamma(\tau \to \mu\nu\bar{\nu})/\Gamma(\tau \to e\nu\bar{\nu})$ for $X = \ell$.[6] Leptonic W-boson decays can also be used to derive constraints on the ratios of leptonic gauge couplings as in $g^W_{\mu/e} \equiv (g_\mu/g_e)^W$ and $g^W_{\tau/\mu} \equiv (g_\tau/g_\mu)^W$; still, we do not list them in the table, as the corresponding bounds are merely weaker versions of other constraints. We similarly have

$$g^X_{\tau/\mu} \equiv \left(\frac{g_\tau}{g_\mu}\right)^X \approx 1 + 0.06\left(\hat{C}^{(3)}_{HL,33} - \hat{C}^{(3)}_{HL,22}\right), \tag{41}$$

where $(g_\tau/g_\mu)^X$ is the ratio of leptonic gauge couplings extracted from the ratio $\Gamma(\tau \to e\nu\bar{\nu})/\Gamma(\mu \to e\nu\bar{\nu})$ for $X = \ell$, and $\Gamma(\tau \to \pi\nu)/\Gamma(\pi \to \mu\nu)$ for $X = \pi$.

In our Seesaw models the predicted deviation of the considered LFU ratios from 1 is at leading order proportional to $\pm(|\theta_\mu|^2 - |\theta_j|^2)$ where $j = e$ or τ, and the sign depends on j as well as which Seesaw model is considered, see Table 6. The derived constraints therefore give rise to hyperbolic contours in the figures presented in this section. Clearly, if the data favours a ratio to be, say, smaller than 1, predicting it to be larger than 1 will lead to a tighter constraint. This then translates into one of the mixing angles being slightly more stringently bounded than another one, with the roles reversed

[6] The flavour of the neutrinos produced in all these decays is assumed to coincide with the one of the respective associated charged lepton, which allows for interference with the SM and can thus be expected to represent the channel dominantly affected by BSM physics.

Table 6 Current constraints on and model predictions for the LFU ratios taken into account in this work. For $R(V_{us})$, the given experimental value refers to the case of $N_f = 2+1+1$ dynamical quark flavours in the lattice simulations from which the relevant decay constants are extracted. The case of $N_f = 2+1$ quark flavours gives rise to a less competitive bound [98]. The model predictions are obtained from matching onto SMEFT at the Seesaw scale $\mu = M^X = 1\,\text{TeV}$ and running to the electroweak scale $\mu = m_Z$. In the right column, the upper sign refers to Type-I Seesaw, whereas the lower sign stands for Type-III Seesaw

Lepton Flavour Universality		
Observable	Measurement	Model prediction
$g^{\pi}_{\mu/e}$	1.0010 ± 0.0009 [100]	$1 \pm 0.48(\lvert\theta_e\rvert^2 - \lvert\theta_\mu\rvert^2)$
$g^{\ell}_{\mu/e}$	1.0017 ± 0.0016 [100]	$1 \pm 0.48(\lvert\theta_e\rvert^2 - \lvert\theta_\mu\rvert^2)$
$g^{K}_{\mu/e}$	0.9978 ± 0.0018 [100]	$1 \pm 0.48(\lvert\theta_e\rvert^2 - \lvert\theta_\mu\rvert^2)$
$R(K_{\ell 3})$	1.001295 ± 0.002891 [101]	$1 \pm 0.48(\lvert\theta_e\rvert^2 - \lvert\theta_\mu\rvert^2)$
$g^{\pi}_{\tau/\mu}$	0.9965 ± 0.0026 [100]	$1 \pm 0.48(\lvert\theta_\mu\rvert^2 - \lvert\theta_\tau\rvert^2)$
$g^{\ell}_{\tau/\mu}$	1.0011 ± 0.0014 [100]	$1 \pm 0.48(\lvert\theta_e\rvert^2 - \lvert\theta_\mu\rvert^2)$
$R(V_{us})$	0.98898 ± 0.00606 [98]	$1 \pm 0.47\lvert\theta_e\rvert^2 \pm 8.80\lvert\theta_\mu\rvert^2 \mp 0.04\lvert\theta_\tau\rvert^2$

if the other Seesaw model is considered. Consequently, if the contribution from a specific mixing angle accommodates the data well in one model, the other model will necessarily increase the tension with the SM.

3.3.2 Light quark mixing

In Table 6 we furthermore consider ratios of the CKM-matrix element V_{us} extracted from the semi-leptonic kaon decays $K_{\mu 3}$ and K_{e3}, the leptonic kaon decay $K_{\mu 2}$, and nuclear beta decay – these are

$$R(K_{\ell 3}) \equiv \frac{V_{us}^{K_{\mu 3}}}{V_{us}^{K_{e3}}} \quad \text{and} \quad R(V_{us}) \equiv \frac{V_{us}^{K_{\mu 2}}}{V_{us}^{\beta}}. \tag{42}$$

The dependence of $R(K_{\ell 3})$ on new physics is identical to that of $g^{\pi}_{\mu/e}$ and $g^{K}_{\mu/e}$, of which both can similarly be viewed as CKM ratios, with the latter being commonly denoted by $R(K_{\ell 2})$. In the following we illustrate why $R(V_{us})$ is a special case, and refer the reader to Ref. [102], wherein the ratio was originally proposed, for further information.

The extracted value of V_{us} from the leptonic kaon decay $K_{\mu 2}$ is

$$V_{us}^{K_{\mu 2}} = V_{us}\left(1 + v_T^2 C^{(3)}_{HL,22} - \frac{\delta \hat{G}_F}{G_F}\right), \tag{43}$$

where V_{us} is a Lagrangian parameter, the $C^{(3)}_{HL,22}$ is due to the new direct contribution, Eq. (39), and $\delta\hat{G}_F/G_F$ parameterises the shift in the Fermi constant. Similarly, beta decay results in

$$V_{ud}^{\beta} = V_{ud}\left(1 + v_T^2 C^{(3)}_{HL,11} - \frac{\delta \hat{G}_F}{G_F}\right), \tag{44}$$

which, as per Ref. [102], is translated to V_{us}^{β} using CKM unitarity of the Lagrangian parameters:

$$\begin{aligned} V_{us}^{\beta} &= \sqrt{1 - |V_{ud}^{\beta}|^2 - |V_{ub}|^2} \\ &\approx V_{us}\left[1 - \left(\frac{V_{ud}}{V_{us}}\right)^2 \left(v_T^2 C^{(3)}_{HL,11} - \frac{\delta \hat{G}_F}{G_F}\right)\right]. \end{aligned} \tag{45}$$

From this we derive the ratio

$$\begin{aligned} R(V_{us}) = \frac{V_{us}^{K_{\mu 2}}}{V_{us}^{\beta}} &= 1 + v_T^2 C^{(3)}_{HL,22} - \frac{\delta \hat{G}_F}{G_F} \\ &\quad + \left(\frac{V_{ud}}{V_{us}}\right)^2 \left(v_T^2 C^{(3)}_{HL,11} - \frac{\delta \hat{G}_F}{G_F}\right) \\ &\approx 1 - v_T^2 \left[\left(\frac{V_{ud}}{V_{us}}\right)^2 C^{(3)}_{HL,22} + C^{(3)}_{HL,11}\right]. \end{aligned} \tag{46}$$

As is explained in Ref. [102], a crucial feature of $R(V_{us})$ is the enhanced sensitivity to new physics due to $(V_{ud}/V_{us})^2 \approx 20$. Experimental data favours the ratio to be smaller than 1 with a significance between 1σ and 2σ, depending on the number of quark flavours assumed for the calculation of the relevant decay constant, see also Table 6.

3.3.3 Discussion

In Fig. 4, the constraints arising from LFU ratios are illustrated. Among those, $R(V_{us})$ is very sensitive to muon mixing and highly relevant for the fermionic Seesaw models. For Type-I Seesaw, the ratio is enhanced and thus driven further away from the data. In fact, $R(V_{us})$ is in conflict with any visible effect in Higgsstrahlung induced via electron or muon mixing, even more so than s_w. The next-to-most competitive

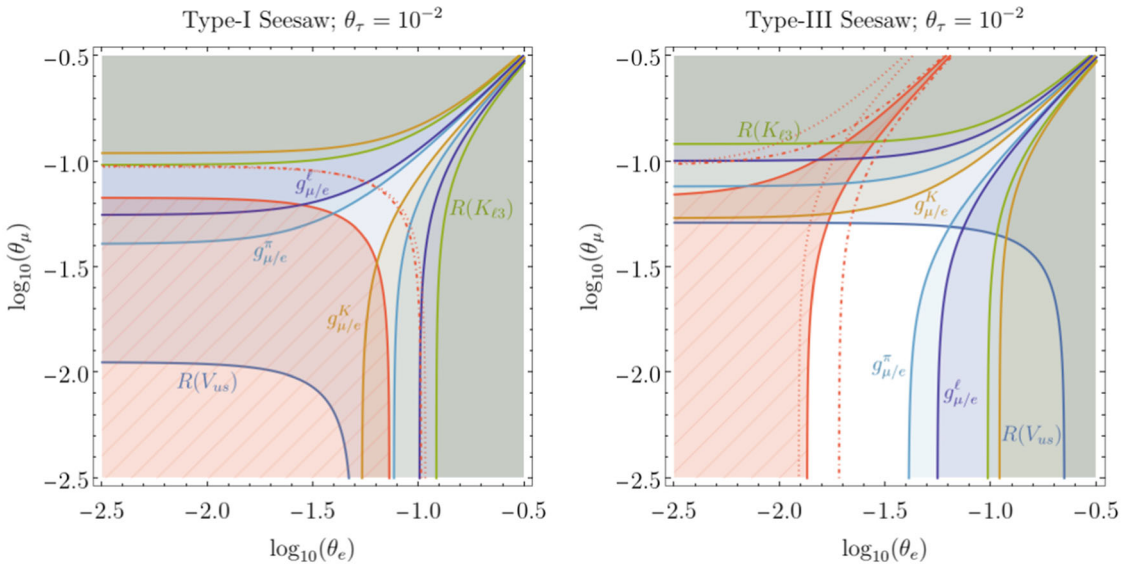

(a) LFU constraints in the θ_e–θ_μ plane.

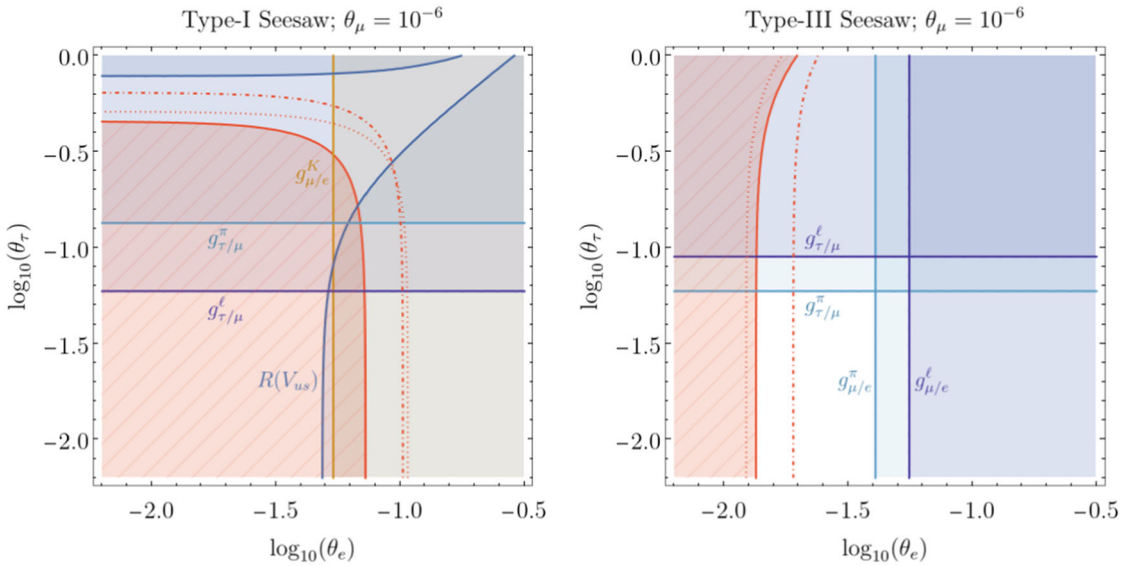

(b) LFU constraints in the θ_e–θ_τ plane. To avoid clutter, subdominant constraints like the one from $R(K_{\ell 3})$ are not drawn, but their locations may be inferred from the above plots.

Fig. 4 Current constraints arising from LFU ratios at 2σ in comparison with projected sensitivities of precision Higgsstrahlung measurements. The red-ruled regions indicate $|\Delta\sigma/\sigma| < 0.5\%$ at $\sqrt{s} = 240\,\text{GeV}$. The dot-dashed and dotted red lines are the corresponding 1% contours at $\sqrt{s} = 240\,\text{GeV}$ and 365 GeV, respectively

bounds on electron and muon mixing arise from $g^K_{\mu/e}$ and $g^\pi_{\mu/e}$, respectively.

In the case of Type-III Seesaw, the most important constraints stem from $g^\pi_{\mu/e}$ and $R(V_{us})$. Since requiring a discernible deviation in the Higgsstrahlung cross section mainly translates into a lower bound on the electron mixing angle in this model and muon mixing may thus be tuned arbitrarily small, the obtained upper limits on $|\theta_e|$ are more relevant in this context. $g^\pi_{\mu/e}$ demands $|\theta_e| \lesssim 0.04$ at 2σ, unless one allows for larger muon mixing and thus a cancellation, whereupon the maximal electron mixing angle allowed by LFU bounds can be rendered up to 50% larger. $R(V_{us})$ implies $|\theta_\mu| \lesssim 0.05$ at 2σ, which holds largely independently of the value chosen for $|\theta_e|$. Note that in a vein similar to m_W, the bounds from $g^K_{\mu/e}$ and $R(V_{us})$ both constrain muon mixing efficiently enough so that no appreciable cancellations of the contributions to Higgsstrahlung from electron mixing can occur for Type-III Seesaw.

As can be seen in Fig. 4b, LFU data constrains tau mixing to $|\theta_\tau| \lesssim 0.06$ for either Seesaw model, which arises from

$g^{\ell}_{\tau/\mu}$ in Type-I, and $g^{\pi}_{\tau/\mu}$ for Type-III. These constraints can in principle be weakened if $|\theta_\mu|$ is more sizeable; still, large changes are only observed for $\mathcal{O}(0.1)$ muon mixing, a scenario which is nonetheless excluded by other observables. While the contributions to $R(V_{us})$ from electron and tau mixing may cancel, this does not open up parameter space in the Type-I Seesaw model, as tau mixing itself is too constrained.

Further LFU ratios not contained in Table 6 deviate from the SM prediction by (close to) 2σ and thus present moderate anomalies in themselves, see Ref. [100]. Explicitly, $g^{K}_{\tau/\mu}$ is measured to be smaller than 1, while $g^{\ell}_{\tau/e}$ and $g^{W}_{\tau/e}$ exceed the SM expectation. If the models under consideration ought to accommodate the data on $g^{K}_{\tau/\mu}$, one would require large tau mixing in comparison with muon mixing for Type-I Seesaw, with the flavours swapped for Type-III Seesaw. The latter is unlikely to be realised for scenarios which are testable via Higgsstrahlung measurements, as large $\Delta\sigma/\sigma_0$ are likely induced via electron mixing in this model, which then demands muon mixing to be very small due to the bounds arising from LFV, see the following section. Similarly, for Type-III Seesaw, the other two ratios necessitate tau mixing to substantially exceed electron mixing in magnitude, which is not a promising scenario either to be tested in the given context, in particular in light of the bound on $\mathrm{BR}(\tau \to 3e)$.

3.4 Lepton flavour violation

As is generically the case for models of neutrino mass generation, the Seesaw models predict sizeable rates for flavour-violating decays of charged leptons. These processes have not been observed to date and thus impart stringent bounds on the parameter space, which will likely get refined in the near future due to several ongoing or upcoming experiments, see Table 7. The scales relevant for these LFV decays are within the realm of LEFT and thus it is instrumental to discuss them in terms of the contributions to LEFT operators. Since we focus on the comparison with the sensitivities to the Higgsstrahlung process at colliders, we restrict ourselves to observables involving electron-flavoured transitions. A comprehensive investigation of LFV effects in the symmetry-protected Type-I Seesaw model can for instance be found in Ref. [118]. We will relegate the explicit matching conditions used in this section to Appendix B.

3.4.1 Radiative charged-lepton decays

The branching ratios for radiative flavour-violating charged-lepton decays read [119]

$$\mathrm{BR}(\ell_i \to \ell_j \gamma) = \frac{m^3_{\ell_i}}{4\pi\,\Gamma_{\ell_i}} \left(|C_{e\gamma,ij}|^2 + |C_{e\gamma,ji}|^2 \right), \tag{47}$$

with the full decay width Γ_{ℓ_i}. We approximately find

$$\begin{aligned}\mathrm{BR}(\mu \to e\gamma) \approx 7.117 \times 10^6 \Big| & \hat{C}_{eB,12} - 0.55\,\hat{C}_{eW,12} \\ & + \left(1.77\,\hat{C}^{(3)}_{HL,12} - 0.48\,\hat{C}^{(1)}_{HL,12}\right) 10^{-6} \Big|^2, \end{aligned} \tag{48}$$

$$\begin{aligned}\mathrm{BR}(\tau \to e\gamma) \approx 0.004 \times 10^6 \Big| & \hat{C}_{eB,13} - 0.55\,\hat{C}_{eW,13} \\ & + \left(29.69\,\hat{C}^{(3)}_{HL,13} - 8.12\,\hat{C}^{(1)}_{HL,13}\right) 10^{-6} \Big|^2, \end{aligned} \tag{49}$$

where the SMEFT Wilson coefficients on the right are evaluated at the electroweak scale $\mu = m_Z$. In both Seesaw models the one-loop matching contributions to the electromagnetic dipole operator $\mathcal{O}_{e\gamma}$ from the electroweak dipole operators $\mathcal{O}_{eB}$ and $\mathcal{O}_{eW}$ are of the same order of magnitude as the contributions from $\mathcal{O}^{(1)}_{HL}$ and $\mathcal{O}^{(3)}_{HL}$ which originate from RG running, see also Eq. (79) in Appendix B.

3.4.2 Trilepton decays

The branching ratio for trilepton decays with identical flavours in the final state is given by [120][7]

$$\begin{aligned}\mathrm{BR}(\ell_i \to \ell_j \ell_j \overline{\ell_j}) = \frac{m^5_{\ell_i}}{3(16\pi)^3\Gamma_{\ell_i}} \Bigg[& 64 \left| C^{VLL}_{ee,jijj} \right|^2 \\ & + 64 \left| C^{VRR}_{ee,jijj} \right|^2 + 8 \left| C^{VLR}_{ee,jijj} \right|^2 + 8 \left| C^{VLR}_{ee,jjji} \right|^2 \\ & + \frac{256e^2}{m^2_{\ell_i}} \left(\ln \frac{m^2_{\ell_i}}{m^2_{\ell_j}} - \frac{11}{4} \right) \left(\left| C^{ij}_{e\gamma} \right|^2 + \left| C^{ji}_{e\gamma} \right|^2 \right) \\ & - \frac{64e}{m_{\ell_i}} \Re \Big[\left(4\,C^{VLL}_{ee,jijj} + C^{VLR}_{ee,jijj} \right) C^{ji*}_{e\gamma} \\ & + \left(4\,C^{VRR}_{ee,jijj} + C^{VLR}_{ee,jjji} \right) C^{ij}_{e\gamma} \Big] \Bigg]. \end{aligned} \tag{50}$$

In the Type-III Seesaw model, these decays are dominated by the vector operators $\mathcal{O}^{VLL}_{ee}$ and $\mathcal{O}^{VLR}_{ee}$, with the flavour change occurring in the left-handed lepton bilinear. These operators receive large contributions from tree-level matching of the Type-III Seesaw model onto SMEFT, and then onto LEFT (see Appendix B). By neglecting all Wilson coefficients apart from $C^{VLX}_{ee,jijj}$ with $X = L, R$, we thus find

$$\begin{aligned}\mathrm{BR}(\mu \to 3e) \approx 1.2 \times 10^{-4} & \\ & \Big[64 \left| 0.27 \left(\hat{C}^{(1)}_{HL,12} + \hat{C}^{(3)}_{HL,12} \right) \right|^2 \\ & + 8 \left| 0.49 \left(\hat{C}^{(1)}_{HL,12} + \hat{C}^{(3)}_{HL,12} \right) \right|^2 \Big] \\ \mathrm{BR}(\tau \to 3e) \approx 0.2 \times 10^{-4} & \end{aligned} \tag{51}$$

[7] See also [119,121] for earlier work. In the case of τ decays, we do not expect significantly more stringent constraints if some of the final-state electrons are swapped for muons.

Table 7 Current and projected constraints on the LFV observables taken into account in this work, together with the pertinent model predictions. The current bounds hold at 90% C.L. The future reach listed for $\mathrm{BR}(\mu \to 3e)$ refers to Phase II of the Mu3e experiment; an initial sensitivity of $\mathrm{BR}(\mu \to 3e) \lesssim 2 \times 10^{-15}$ is expected after Phase I. The upper (lower) value listed for the future reach of $\mathrm{CR}(\mu - e; \mathrm{Al})$ refers to COMET (Mu2e). The model predictions are obtained from matching onto SMEFT at the Seesaw scale $\mu = M^X = 1\,\mathrm{TeV}$, running to the electroweak scale $\mu = m_Z$, matching onto LEFT and running to the low scale $\mu = 5\,\mathrm{GeV}$

Lepton flavour violation						
Observable	Experiment				Model predictions	
	Current bound		Future reach		Type-I	Type-III
$\mathrm{BR}(\mu \to e\gamma)$	4.2×10^{-13}	[104]	6×10^{-14}	[105]	$0.82 \times 10^{-3}\,\lvert\theta_e\theta_\mu\rvert^2$	$1.27 \times 10^{-3}\,\lvert\theta_e\theta_\mu\rvert^2$
$\mathrm{BR}(\mu \to 3e)$	1×10^{-12}	[106]	1×10^{-16}	[107]	$0.14 \times 10^{-3}\,\lvert\theta_e\theta_\mu\rvert^2$	$0.72\,\lvert\theta_e\theta_\mu\rvert^2$
$\mathrm{CR}(\mu - e; \mathrm{Au})$	7×10^{-13}	[108]	–		$0.04 \times 10^{-3}\,\lvert\theta_e\theta_\mu\rvert^2$	$27.1\,\lvert\theta_e\theta_\mu\rvert^2$
$\mathrm{CR}(\mu - e; \mathrm{Al})$	–		2.6×10^{-17}	[109]	$0.15 \times 10^{-3}\,\lvert\theta_e\theta_\mu\rvert^2$	$6.7\,\lvert\theta_e\theta_\mu\rvert^2$
			8×10^{-17}	[110]		
$\mathrm{CR}(\mu - e; \mathrm{Ti})$	6.1×10^{-13}	[111]	$\mathcal{O}(10^{-18})$	[112]	$0.18 \times 10^{-3}\,\lvert\theta_e\theta_\mu\rvert^2$	$13.5\,\lvert\theta_e\theta_\mu\rvert^2$
$\mathrm{CR}(\mu - e; \mathrm{Pb})$	4.6×10^{-11}	[113]	–		$0.02 \times 10^{-3}\,\lvert\theta_e\theta_\mu\rvert^2$	$20.3\,\lvert\theta_e\theta_\mu\rvert^2$
$\mathrm{CR}(\mu - e; \mathrm{S})$	7×10^{-11}	[114]	–		$0.21 \times 10^{-3}\,\lvert\theta_e\theta_\mu\rvert^2$	$6.4\,\lvert\theta_e\theta_\mu\rvert^2$
$\mathrm{BR}(\tau \to e\gamma)$	3.3×10^{-8}	[115]	9×10^{-9}	[116]	$0.15 \times 10^{-3}\,\lvert\theta_e\theta_\tau\rvert^2$	$0.23 \times 10^{-3}\,\lvert\theta_e\theta_\tau\rvert^2$
$\mathrm{BR}(\tau \to 3e)$	2.7×10^{-8}	[117]	4.7×10^{-10}	[116]	$0.02 \times 10^{-3}\,\lvert\theta_e\theta_\tau\rvert^2$	$0.13\,\lvert\theta_e\theta_\tau\rvert^2$

$$\Big[64\left|0.27\Big(\hat{C}^{(1)}_{HL,13}+\hat{C}^{(3)}_{HL,13}\Big)\right|^2 + 8\left|0.49\Big(\hat{C}^{(1)}_{HL,13}+\hat{C}^{(3)}_{HL,13}\Big)\right|^2\Big], \tag{52}$$

where the SMEFT Wilson coefficients on the right are evaluated at the electroweak scale $\mu = m_Z$. In the Type-I Seesaw model, all Wilson coefficients entering the branching ratios for trilepton decays receive contributions from matching onto SMEFT only at loop level. In this case, the branching ratios are relatively more sensitive to the contributions from the electromagnetic dipole operator $\mathcal{O}_{e\gamma}$, and the above approximations are only accurate to about 20%.

3.4.3 $\mu - e$ conversion in nuclei

As the scalar and gluon operators are suppressed in the fermionic Seesaw models, the $\mu - e$ conversion rate takes the simple form [122,123]

$$\omega_{\mathrm{conv}} = \left|-\frac{C_{e\gamma,12}}{2m_\mu}D + \tilde{g}^{(p)}_{LV}V^{(p)} + \tilde{g}^{(n)}_{LV}V^{(n)}\right|^2 + \left|-\frac{C^*_{e\gamma,21}}{2m_\mu}D + \tilde{g}^{(p)}_{RV}V^{(p)} + \tilde{g}^{(n)}_{RV}V^{(n)}\right|^2, \tag{53}$$

where the overlap integrals D, $V^{(p)}$ and $V^{(n)}$, and muon capture rates ω_{capt} can be found in Refs. [122,124], and the effective coupling constants are

$$\tilde{g}^{(p)}_{LV} = 2\left(C^{VLL}_{eu,1211}+C^{VLR}_{eu,1211}\right) + \left(C^{VLL}_{ed,1211}+C^{VLR}_{ed,1211}\right), \tag{54}$$

$$\tilde{g}^{(p)}_{RV} = 2\left(C^{VRR}_{eu,1211}+C^{VLR}_{ue,1112}\right) + \left(C^{VRR}_{ed,1211}+C^{VLR}_{de,1112}\right), \tag{55}$$

$$\tilde{g}^{(n)}_{LV} = \left(C^{VLL}_{eu,1211}+C^{VLR}_{eu,1211}\right) + 2\left(C^{VLL}_{ed,1211}+C^{VLR}_{ed,1211}\right), \quad \text{and} \tag{56}$$

$$\tilde{g}^{(n)}_{RV} = \left(C^{VRR}_{eu,1211}+C^{VLR}_{ue,1112}\right) + 2\left(C^{VRR}_{ed,1211}+C^{VLR}_{de,1112}\right); \tag{57}$$

see Appendix B for approximate matching expressions.

We are interested in the conversion ratio $\mathrm{CR}(\mu \to e)$, defined as the ratio of the $\mu - e$ conversion rate ω_{conv} over the muon capture rate ω_{capt}. For the Type-I and Type-III Seesaw models it approximates to

$$\mathrm{CR}(\mu \to e) \approx \left(\frac{m_\mu}{\mathrm{GeV}}\right)^5 \begin{Bmatrix} 5.87 \\ 1.16 \\ 21.54 \end{Bmatrix} \times 10^5 \left|\left[2\left(\hat{C}^{VLL}_{eu,1211}+\hat{C}^{VLR}_{eu,1211}\right) + \left(\hat{C}^{VLL}_{ed,1211}+\hat{C}^{VLR}_{ed,1211}\right)\right]\begin{Bmatrix} 0.0396 \\ 0.0974 \\ 0.0161 \end{Bmatrix} + \left[\left(\hat{C}^{VLL}_{eu,1211}+\hat{C}^{VLR}_{eu,1211}\right) + 2\left(\hat{C}^{VLL}_{ed,1211}+\hat{C}^{VLR}_{ed,1211}\right)\right]\begin{Bmatrix} 0.0468 \\ 0.146 \\ 0.0173 \end{Bmatrix}\right|^2, \tag{58}$$

where the Wilson coefficients on the right are evaluated at the low scale $\mu = 5\,\text{GeV}$, and where the upper, middle and lower entry in the brackets refers to a titanium (Ti), gold (Au) and aluminium (Al) target, respectively. We also include the predictions for the conversion ratios for lead (Pb) and sulfur (S) in Table 7, from which one can infer that the respective current bounds do not impose relevant constraints. As is reflected by the above approximation, $\mu - e$ conversion is dominated by contributions from left-handed vector operators in both Seesaw models. This is evident in Type-III where these contributions are sourced at tree level, but also holds in Type-I. The electroweak dipole operator $\mathcal{O}_{e\gamma,12}$ plays a subdominant role in both models.

3.4.4 Discussion

We find that for the Type-I Seesaw model, as per the absence of tree-level contributions to trilepton decays and $\mu - e$ conversion, the most competitive bounds currently arise from the non-observation of $\mu \to e\gamma$ and $\tau \to e\gamma$, see Fig. 5. Therefore, a detectable shift in $\sigma(e^+e^- \to Zh)$ would enforce either $|\theta_e| \gtrsim 0.1$ and $|\theta_\mu| \lesssim 10^{-4}$, or vice versa. Still, in the $\mu - e$ sector, we expect the limits from $\text{BR}(\mu \to 3e)$ and $\text{CR}(\mu - e)$ to become more stringent in the future, and further improve this bound by up to two orders of magnitude. The relatively loose current bound from $\text{CR}(\mu - e;\ \text{Au})$ is due to cancellations between the effective vector couplings to protons and neutrons. These generically occur for all target materials in both fermionic Seesaw models, but are insignificant for Type-III. In the case of Type-I, matching at a larger scale reduces the cancellations for $\text{CR}(\mu - e;\ \text{Au})$, cf. Sect. 3.5. See also for instance Ref. [125] for a pertinent discussion. Currently, the non-observation of $\tau \to e\gamma$ enforces $|\theta_\tau| \lesssim 0.1$ for $|\theta_e| \gtrsim 0.1$, and $|\theta_e| \lesssim 0.02$ for $|\theta_\tau| \gtrsim 0.6$. These limits can be expected to become slightly more stringent in light of the future reaches of $\text{BR}(\tau \to e\gamma)$ and $\text{BR}(\tau \to 3e)$, still, the improvements are expected to be less than an order of magnitude.

In Type-III Seesaw, due to tree-level contributions to the respective pertinent operators, the bounds from $\text{BR}(\mu \to 3e)$ and $\text{CR}(\mu - e)$ are stricter than that of $\text{BR}(\mu \to e\gamma)$, and $\tau \to 3e$ is also more competitive than $\tau \to e\gamma$. Note that the projected sensitivity to $\text{BR}(\mu \to e\gamma)$ at MEG II cannot even be expected to supersede the current bound on $\text{BR}(\mu \to 3e)$. Moreover, the existing bound on $\mu - e$ conversion in gold effectively enforces the muon mixing angle to be smaller than $|\theta_\mu| \lesssim 10^{-5}$ for $|\theta_e| > 10^{-2}$ which is required for an observable deviation of the Higgsstrahlung cross section at a future lepton collider. Thus, the measurements of the cross section are only sensitive to a rather pronounced hierarchy $|\theta_\mu/\theta_e| \lesssim 10^{-3}$. A hierarchy $|\theta_e/\theta_\mu| \lesssim 10^{-5}$, corresponding to the region visible in the top-left of Fig. 5a, is in principle also compatible with the LFV bounds, but still disfavoured by the constraints from electroweak and LFU observables, see the relevant sections above.

Similarly, the non-observation of $\tau \to 3e$ presently constrains the tau mixing angle to $|\theta_\tau| \lesssim 0.03$ if a non-SM signature in $\sigma(e^+e^- \to Zh)$ is to be attainable, that is, tau mixing should not substantially exceed electron mixing in magnitude. This limit on $|\theta_\tau|$ would be strengthened by an order of magnitude if no decay $\tau \to 3e$ is observed at Belle II, which will then also necessitate a hierarchy $|\theta_\tau/\theta_e| \lesssim 0.1$ if a chance of detecting $\Delta\sigma/\sigma_0$ is to be retained. In a similar vein, if no signals in $\mu \to 3e$ or $\mu - e$ conversion in aluminium are observed in the future, the ratio of the relevant mixing angles will be constrained to be even as small as $|\theta_\mu/\theta_e| \lesssim 10^{-4}$ or 10^{-5}, respectively.

3.5 Larger Seesaw scale

Lastly, we will comment on the scenario with a larger matching scale. In Table 8 we have collected our results for the shifts in the observables considered in our work for the Seesaw scale $\mu = M^X = 10\,\text{TeV}$.

In the case of the Type-III Seesaw model, we find that the results discussed in this section seem to be fairly robust with respect to raising the triplet mass to $\mathcal{O}(10\,\text{TeV})$ at least. That is, the numerical coefficients entering the expressions for the considered observables typically change by less than 20%. The only notable differences lie in the sensitivity of δm_W and $\Delta\sigma/\sigma_0$ to tau-flavour mixing at larger centre-of-mass energies, where the respective coefficients grow by a factor of 2–5. Still, it is a subleading effect, as these observables remain much more sensitive to electron- and muon-flavour mixing. Therefore, the results for the Type-III Seesaw model discussed in Sect. 3 so far, for which $M^\Sigma = 1\,\text{TeV}$ is assumed, will also approximately hold for (moderately) larger masses.

In contrast, the observable phenomenology of Type-I Seesaw morphs somewhat nontrivially upon raising the Seesaw scale to $M^\nu = \mathcal{O}(10\,\text{TeV})$. Most profoundly, the Higgsstrahlung shift $\Delta\sigma/\sigma_0$ now experiences a crossing near $\sqrt{s} = 500\,\text{GeV}$, whereupon the dependence on the squared electron mixing angle $|\theta_e|^2$ reverses from positive to negative. Additionally, the trilepton decay rates receive a relative numerical boost of 200%, and the $\mu - e$ conversion rates are, in general, significantly altered. Specifically, $\mu - e$ conversion in gold and lead increase substantially due to the fact that the effective left-handed vector couplings to neutrons increase by a factor larger than 2, while the proton couplings and the dipole operator remain largely unchanged and thus the cancellations are much less efficient. On the contrary, $\mu - e$ conversion in aluminium and titanium experience a suppression. This implies in particular that the cur-

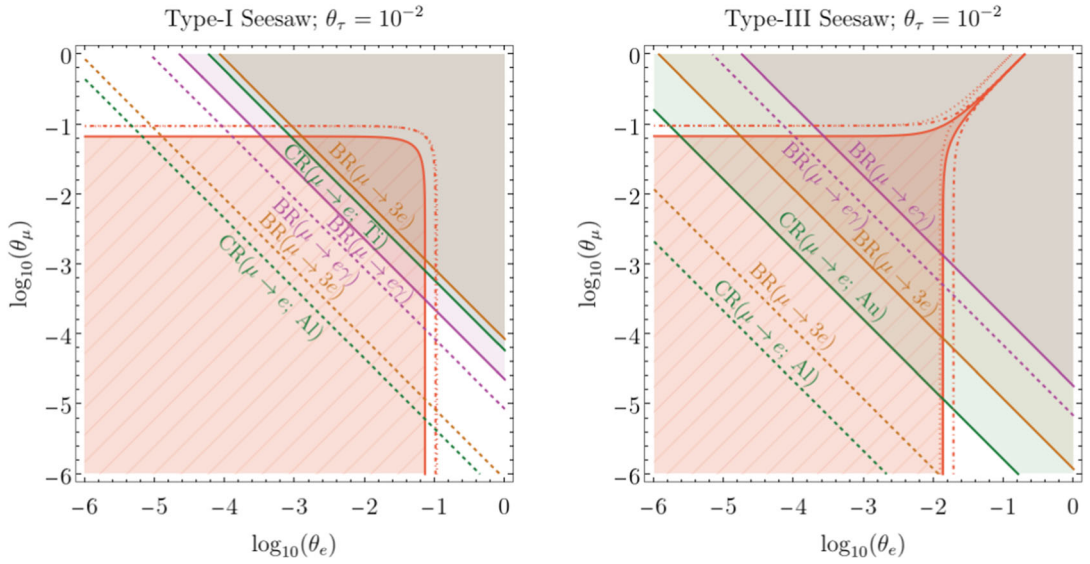

(a) LFV constraints in the θ_e–θ_μ plane. Though we checked the current bounds arising from $\mu - e$ conversion for different target materials, here we display only the most competitive ones for each model, respectively. The PRISM/PRIME [112] proposal may even further extend the new-physics reach of $\mu - e$ conversion.

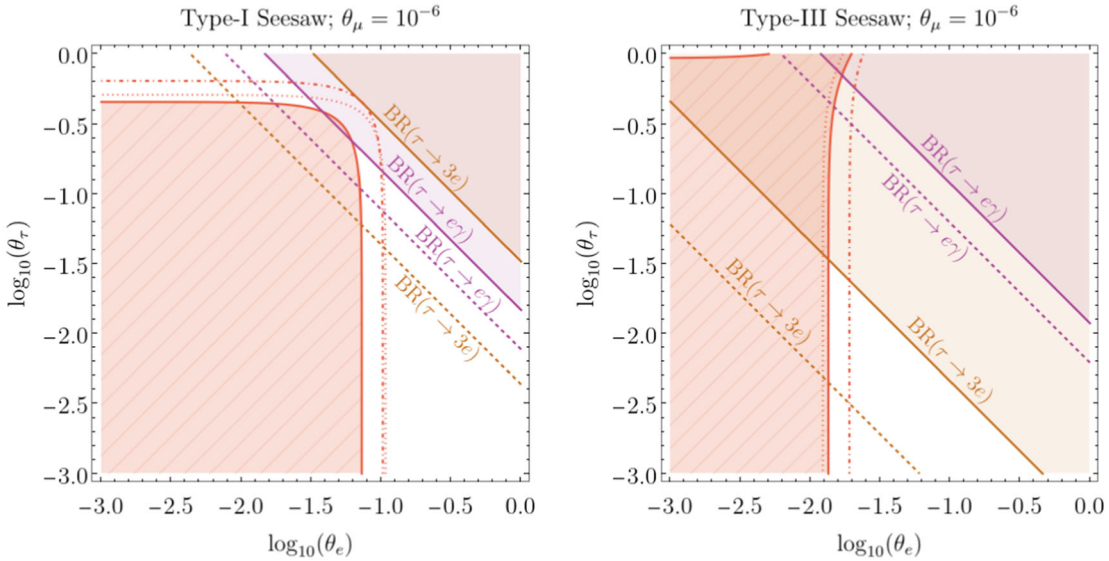

(b) LFV constraints in the θ_e–θ_τ plane.

Fig. 5 Current constraints from LFV observables depicted at 90% C.L., together with their prospective future reaches, in comparison with projected sensitivities of precision Higgsstrahlung measurements. The red-ruled regions indicate $|\Delta\sigma/\sigma| < 0.5\%$ at $\sqrt{s} = 240\,\text{GeV}$. The dot-dashed and dotted red lines are the corresponding 1% contours at $\sqrt{s} = 240\,\text{GeV}$ and 365 GeV, respectively. We do not depict the bounds from tau-flavoured processes in the θ_e–θ_μ plots, and vice versa. If included, they would appear as vertical lines with positioning highly dependent on the choice of the third mixing angle, which limits their relevance

rent bound arising from $\mu - e$ conversion in gold is clearly stronger than the one from titanium, unlike the scenario with $M^\nu = 1\,\text{TeV}$.

4 Summary

We have computed the correction to the tree-level cross section of the Higgsstrahlung process $e^+e^- \to Zh$ in the LN-conserving limit of the Type-I and Type-III Seesaw models, and compared several benchmark sensitivities of next-generation lepton colliders to existing and prospective con-

Table 8 Contributions to the observables considered in the phenomenology study in this work, but obtained from matching onto SMEFT at a Seesaw scale $\mu = M^X = 10\,\text{TeV}$

	Type-I	Type-III
$\Delta\sigma/\sigma_0$ (240 GeV)	$0.74\,\lvert\theta_e\rvert^2 + 1.11\,\lvert\theta_\mu\rvert^2 + 0.06\,\lvert\theta_\tau\rvert^2$	$26.30\,\lvert\theta_e\rvert^2 - 1.07\,\lvert\theta_\mu\rvert^2 - 0.01\,\lvert\theta_\tau\rvert^2$
$\Delta\sigma/\sigma_0$ (365 GeV)	$0.41\,\lvert\theta_e\rvert^2 + 1.18\,\lvert\theta_\mu\rvert^2 + 0.12\,\lvert\theta_\tau\rvert^2$	$63.12\,\lvert\theta_e\rvert^2 - 1.09\,\lvert\theta_\mu\rvert^2 - 0.03\,\lvert\theta_\tau\rvert^2$
$\Delta\sigma/\sigma_0$ (500 GeV)	$-0.05\,\lvert\theta_e\rvert^2 + 1.26\,\lvert\theta_\mu\rvert^2 + 0.19\,\lvert\theta_\tau\rvert^2$	$120.66\,\lvert\theta_e\rvert^2 - 1.11\,\lvert\theta_\mu\rvert^2 - 0.05\,\lvert\theta_\tau\rvert^2$
δs_w^2	$-0.151(\lvert\theta_e\rvert^2 + \lvert\theta_\mu\rvert^2) + 0.005\,\lvert\theta_\tau\rvert^2$	$0.021(\lvert\theta_e\rvert^2 + \lvert\theta_\mu\rvert^2) - 0.135\,\lvert\theta_\tau\rvert^2$
δm_W/GeV	$7.95(\lvert\theta_e\rvert^2 + \lvert\theta_\mu\rvert^2) - 0.24\,\lvert\theta_\tau\rvert^2$	$-8.44(\lvert\theta_e\rvert^2 + \lvert\theta_\mu\rvert^2) - 0.24\,\lvert\theta_\tau\rvert^2$
$g^X_{\mu/e}$	$1 + 0.47(\lvert\theta_e\rvert^2 - \lvert\theta_\mu\rvert^2)$	$1 - 0.47(\lvert\theta_e\rvert^2 - \lvert\theta_\mu\rvert^2)$
$g^X_{\tau/\mu}$	$1 + 0.47(\lvert\theta_\mu\rvert^2 - \lvert\theta_\tau\rvert^2)$	$1 - 0.47(\lvert\theta_\mu\rvert^2 - \lvert\theta_\tau\rvert^2)$
$R(V_{us})$	$1 + 0.44\,\lvert\theta_e\rvert^2 + 8.58\,\lvert\theta_\mu\rvert^2 - 0.07\,\lvert\theta_\tau\rvert^2$	$1 - 0.44\,\lvert\theta_e\rvert^2 - 8.58\,\lvert\theta_\mu\rvert^2 + 0.07\,\lvert\theta_\tau\rvert^2$
$\text{BR}(\mu \to e\gamma)$	$0.80 \times 10^{-3}\,\lvert\theta_e\theta_\mu\rvert^2$	$1.21 \times 10^{-3}\,\lvert\theta_e\theta_\mu\rvert^2$
$\text{BR}(\mu \to 3e)$	$0.34 \times 10^{-3}\,\lvert\theta_e\theta_\mu\rvert^2$	$0.66\,\lvert\theta_e\theta_\mu\rvert^2$
$\text{CR}(\mu \to e; \text{Au})$	$0.94 \times 10^{-3}\,\lvert\theta_e\theta_\mu\rvert^2$	$24.7\,\lvert\theta_e\theta_\mu\rvert^2$
$\text{CR}(\mu \to e; \text{Al})$	$0.03 \times 10^{-3}\,\lvert\theta_e\theta_\mu\rvert^2$	$6.1\,\lvert\theta_e\theta_\mu\rvert^2$
$\text{CR}(\mu \to e; \text{Ti})$	$0.15 \times 10^{-3}\,\lvert\theta_e\theta_\mu\rvert^2$	$12.3\,\lvert\theta_e\theta_\mu\rvert^2$
$\text{CR}(\mu \to e; \text{Pb})$	$0.76 \times 10^{-3}\,\lvert\theta_e\theta_\mu\rvert^2$	$18.5\,\lvert\theta_e\theta_\mu\rvert^2$
$\text{CR}(\mu \to e; \text{S})$	$0.01 \times 10^{-3}\,\lvert\theta_e\theta_\mu\rvert^2$	$5.8\,\lvert\theta_e\theta_\mu\rvert^2$
$\text{BR}(\tau \to e\gamma)$	$0.15 \times 10^{-3}\,\lvert\theta_e\theta_\tau\rvert^2$	$0.23 \times 10^{-3}\,\lvert\theta_e\theta_\tau\rvert^2$
$\text{BR}(\tau \to 3e)$	$0.06 \times 10^{-3}\,\lvert\theta_e\theta_\tau\rvert^2$	$0.12\,\lvert\theta_e\theta_\tau\rvert^2$

straints from electroweak precision measurements, and LFU and LFV probes. Summary plots in the θ_e–θ_μ and θ_e–θ_τ planes are presented in Fig. 6.

As a major result, we found that existing data on the effective leptonic weak mixing angle and LFU observables preclude substantial corrections to the Higgsstrahlung cross section for Type-I Seesaw. The most likely signature of this model at a future lepton collider is therefore the *absence* of a detectable deviation from the SM prediction, at least if no further new physics modifying the electroweak and LFU sectors is introduced. For Type-III Seesaw, the current constraints (at 2σ) leave genuinely viable parameter space that can be probed at an e^+e^- Higgs factory. Figure 7 provides a magnified view of this region. Concretely, for a centre-of-mass energy $\sqrt{s} = 240\,\text{GeV}$ the largest permitted shift in the Higgsstrahlung cross section is ∼5%; at $\sqrt{s} = 365\,\text{GeV}$ it is ∼12%.

The viable region in Type-III is isolated by three main considerations. Firstly, the non-observation of LFV tightly constrains any scenario with sizeable mixing of heavy fermion singlets or triplets with two lepton flavours. These constraints are particularly strong for Type-III Seesaw, which induces tree-level contributions to trilepton decays and $\mu - e$ conversion. Indeed, a detectable deviation in $\sigma(e^+e^- \to Zh)$ already necessitates a sizeable hierarchy between θ_e and θ_μ which will become more pronounced if signals of LFV remain elusive in the future. (The situation is similar for Type-I Seesaw, where in the absence of contributions to LFV at tree level, the radiative decays $\mu \to e\gamma$ and $\tau \to e\gamma$ are more important.) Secondly (and thirdly), both the W-boson mass m_W and LFU data currently disfavour detectable corrections induced via muon mixing at the level of 2σ, but leave room for visible effects due to electron-flavoured couplings, which together with the LFV constraints enforces a hierarchy $|\theta_\mu/\theta_e| \lesssim 10^{-3}$.

Focusing on the viable region in Fig. 7, the constraints arising from the LFU ratio $g^\pi_{\mu/e}$ and m_W are similarly competitive and provide the most stringent constraint on electron mixing in the Type-III Seesaw model, with $|\theta_e| \lesssim 0.04$ at 2σ. Note also that in the region of parameter space where $\Delta\sigma/\sigma_0$ is detectable, tau-flavour mixing is more strictly constrained by the current bound on $\text{BR}(\tau \to 3e)$ than by measurements of the weak mixing angle or pion decays. As is expected from Sect. 3.4, the most competitive upper limit on muon mixing in the given context currently arises from the non-observation of $\mu - e$ conversion in gold, and will be further constrained by Mu3e as well as the searches for $\mu - e$ conversion in aluminium at COMET and Mu2e. If an observation of these transitions remains elusive in the future, the currently viable parameter space will retreat to $|\theta_\mu| \lesssim 10^{-7.5}$. Similarly, if $\tau \to 3e$ is not observed at Belle II, tau mixing would need to be smaller than $\theta_\tau = 10^{-2}$.

Since fermion triplets induce a tree-level contribution to $e^+e^- \to Zh$ which is not mediated via the s channel as in the SM, deviations from the cross section induced via electron-flavour mixing grow approximately with s. In that sense, if

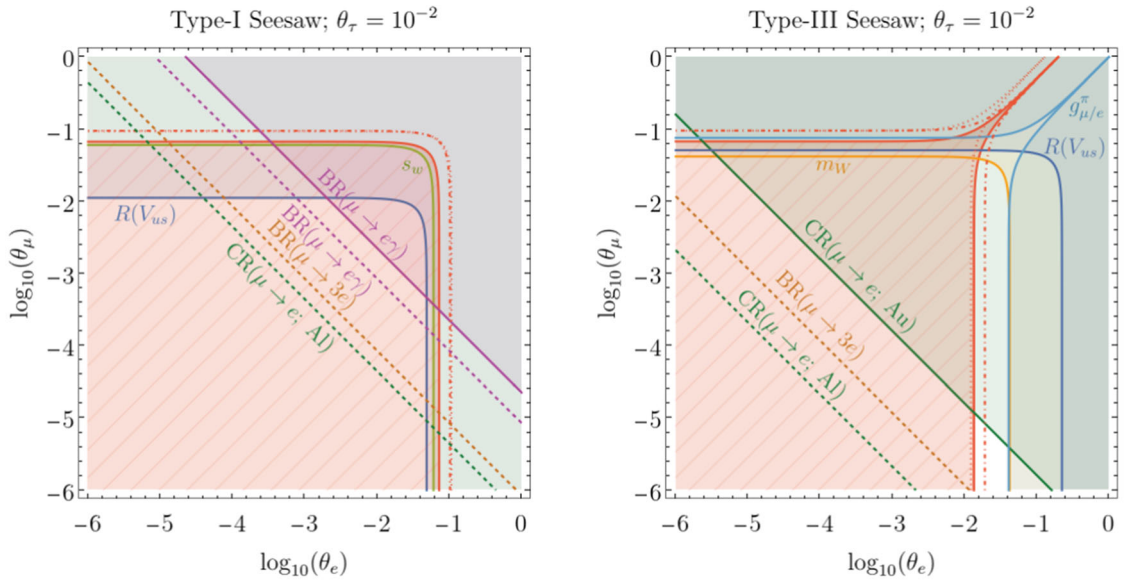

(a) Summary plots in the θ_e–θ_μ plane.

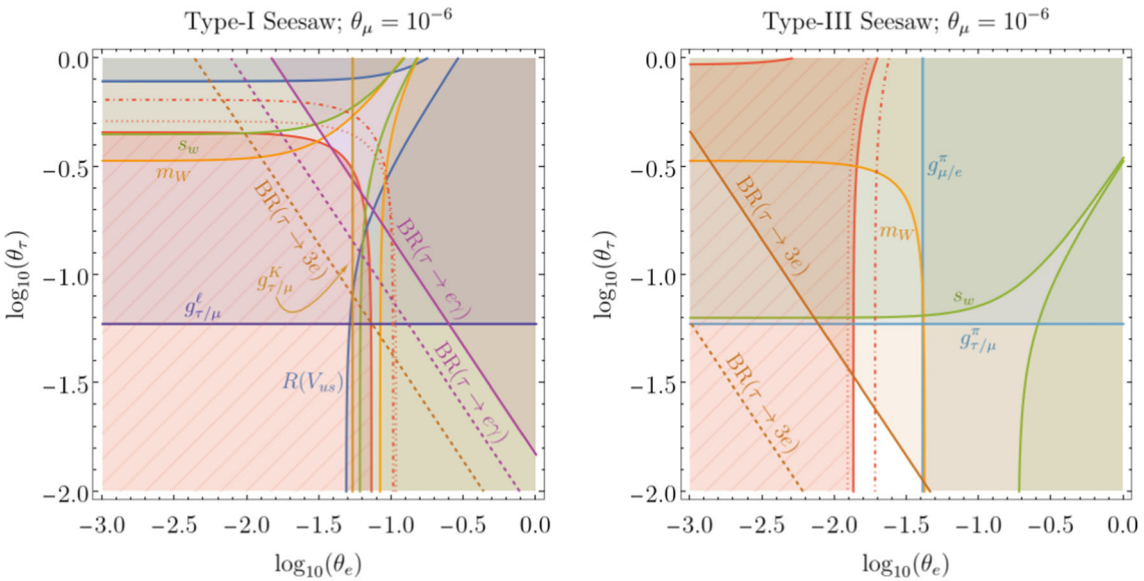

(b) Summary plots in the θ_e–θ_τ plane.

Fig. 6 Summary plots featuring the most competitive current constraints as well as future reaches considered in this work in comparison with projected sensitivities of precision Higgsstrahlung measurements. The red-ruled regions indicate $|\Delta\sigma/\sigma| < 0.5\%$ at $\sqrt{s} = 240\,\mathrm{GeV}$. The dot-dashed and dotted red lines are the corresponding 1% contours at $\sqrt{s} = 240\,\mathrm{GeV}$ and 365 GeV, respectively

the drop in statistics can be compensated by higher luminosity, the Type-III Seesaw model motivates precision measurements of the Higgsstrahlung process at higher centre-of-mass energies as well, whereas this is not indicated for Type-I Seesaw.

Overall, we have corroborated the expectation that a rich interplay of neutrino, Higgs, electroweak and flavour physics is to be expected for Seesaw models at low energies, and demonstrated the benefit of measuring the Higgsstrahlung cross section at multiple centre-of-mass energies for the Type-III Seesaw model. One may extend the research conducted in this work along two major avenues. Firstly, although the list of processes which we consider in the analysis captures a wide range of phenomenology of the fermionic Seesaw models, it is not exhaustive. In particular, taking into account observables sensitive to angular distributions for Higgs physics [126] as well as a comprehensive global fit in the electroweak sector should help to further differentiate between the low-energy signatures of Seesaw models. Secondly, since we relied on the assumption of an

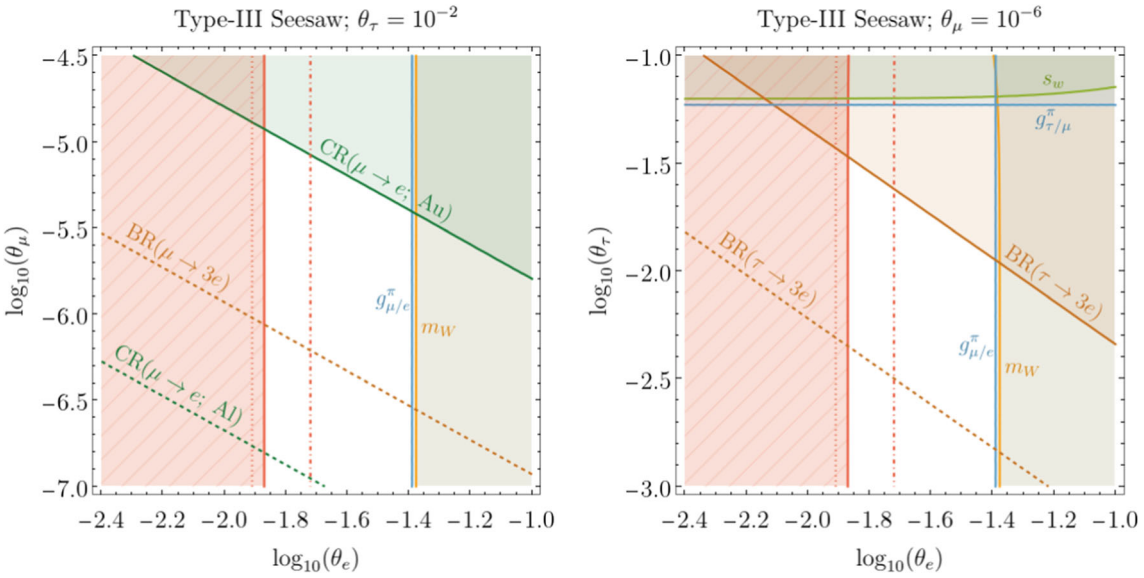

Fig. 7 Plots zoomed in on the viable parameter regions in the Type-III Seesaw model. Only the most constraining observables are depicted. The red-ruled regions indicate $|\Delta\sigma/\sigma| < 0.5\%$ at $\sqrt{s} = 240\,\mathrm{GeV}$. The dot-dashed and dotted red lines are the corresponding 1% contours at $\sqrt{s} = 240\,\mathrm{GeV}$ and 365 GeV, respectively

exactly conserved LN symmetry on the Lagrangian level, existing data on lepton mixing and the mass hierarchies in the neutrino sector was *per definition* not incorporated. While we expect the implications of explicit breakings of lepton number for the induced low-energy phenomenology to be small in general, any viable model of neutrino mass generation eventually needs to be tested against them. Lastly, we leave similar studies for different models of neutrino mass generation for future work.

Acknowledgements We acknowledge support by the Australian Research Council through the ARC Discovery Project DP200101470. AL acknowledges support from an Australian Government Research Training Program Scholarship. TF has also been supported by a UNSW Science PhD Writing Scholarship. The Feynman diagrams in this article were generated using TikZ-Feynman [127].

Data Availability Statement This manuscript has no associated data or the data will not be deposited. [Authors' comment: This is a theoretical study and no new data has been generated. The mathematical expressions in the tables approximately describe the lines shown in the figures.]

Funded by SCOAP[3]. SCOAP[3] supports the goals of the International Year of Basic Sciences for Sustainable Development.

Appendix A: A brief overview of parameter shifts in SMEFT

Here we supplement this work with a somewhat pedagogical overview aimed at explaining how to arrive at the parameter shifts presented in the main text. This overview is not entirely self-contained, and we recommend the reader refer to Section 5 of Ref. [75], which provides an excellent guided tour of much upon which this exposition relies. We will match their notation with the exception of the gauge fields and their couplings, as their redefinition due to $\mathcal{O}_{HW}$ and $\mathcal{O}_{HB}$ is just a matter of bookkeeping. (Practically, this means we will continue to write e.g. g_2 and Z_μ instead of $\bar{g}_2$ and $\mathcal{Z}_\mu$ respectively.) Herein we work to order $(v/\Lambda)^2$, where Λ is the cut-off scale of the effective theory, equal to M^X in the Seesaw models.

Part 1: Effective Parameters

We denote with a bar, e.g. $\bar{g}$, an effective parameter that appears in place of its unbarred form in the SMEFT Lagrangian after all effective operators have been expanded out and the dust settles. For example, the Z-boson part of the gauge-covariant derivative, which in the SM reads

$$D_\mu \supset -i g_Z (T^3 - s_w^2 Q) Z_\mu, \tag{59}$$

becomes in SMEFT

$$D_\mu \supset -i\bar{g}_Z(T^3 - \bar{s}_w^2 Q)Z_\mu, \tag{60}$$

where [75]

$$\bar{g}_Z = \sqrt{g_1^2+g_2^2}\left(1+\frac{g_1 g_2}{g_1^2+g_2^2}v_T^2 C_{HWB}\right), \quad \text{and}$$
$$\bar{s}_w^2 = \frac{g_1^2}{g_1^2+g_2^2}\left(1-\frac{g_2}{g_1}\frac{g_1^2-g_2^2}{g_1^2+g_2^2}v_T^2 C_{HWB}\right). \tag{61}$$

To denote the shifts of these parameters from their SM expressions we write

$$\bar{g}_Z = g_Z + \delta\bar{g}_Z, \quad \text{and} \quad \bar{s}_w^2 = s_w^2 + \delta\bar{s}_w^2, \tag{62}$$

where the corrections are

$$\frac{\delta\bar{g}_Z}{g_Z} = \frac{g_1 g_2}{g_1^2+g_2^2}v_T^2 C_{HWB}, \quad \text{and}$$
$$\frac{\delta\bar{s}_w^2}{s_w^2} = -\frac{g_2}{g_1}\frac{g_1^2-g_2^2}{g_1^2+g_2^2}v_T^2 C_{HWB}. \tag{63}$$

Note that $\delta\bar{g}_Z/g_Z = \delta\bar{g}_Z/\bar{g}_Z$ at order $(v/\Lambda)^2$ (and similarly so for every other parameter), so we will consistently opt to write the former, which uses less ink.

To reiterate the notation and have a referenceable equation, the shift for a general parameter g is written

$$\bar{g} = g + \delta\bar{g}. \tag{64}$$

There is one exception to this notational rule in v_T, which should be written $\bar{v}$ for consistency, but isn't by convention. In this case we have $v_T = v + \delta\bar{v}$.

Part 2: Input Parameters

We denote with a hat, e.g. $\hat{\alpha}$, a parameter directly measured, or derived from measured values using tree-level SM relations. For a parameter directly measured we have

$$\hat{\alpha} = \bar{\alpha} + \delta\hat{\alpha} = \alpha + \delta\bar{\alpha} + \delta\hat{\alpha}. \tag{65}$$

Here there is an additional contribution, labelled $\delta\hat{\alpha}$, which comes from other diagrams contributing to the measurement process, and which cannot be absorbed into a redefinition of the parameter as above. Such diagrams typically arise at the loop order or at $\mathcal{O}(v/\Lambda)^4$, which we neglect, therefore leaving $\delta\hat{\alpha} = 0$. The sole exception to this is the Fermi constant, which acquires tree-level contributions to $\delta\hat{G}_F$ from the diagrams in Fig. 8.

For a parameter computed from the input parameters using the tree-level SM relations, $\hat{g} \equiv g(\hat{\alpha}_i)$ (one such example would be computing the elementary charge from the measured value of the fine structure constant via $\hat{e} = \sqrt{4\pi\hat{\alpha}}$), we instead have

$$\hat{g} = g + \frac{\partial g}{\partial \alpha_i}\left(\delta\bar{\alpha}_i + \delta\hat{\alpha}_i\right) \equiv g + \delta\hat{g}. \tag{66}$$

By combining Eqs. (64) and (66), we see that

$$\bar{g} = \hat{g} + \delta\bar{g} - \delta\hat{g}$$
$$\equiv \hat{g} + \delta g. \tag{67}$$

As will soon become apparent, we will be most interested in computing this total shift,

$$\delta g \equiv \delta\bar{g} - \frac{\partial g}{\partial \alpha_i}\left(\delta\bar{\alpha}_i + \delta\hat{\alpha}_i\right). \tag{68}$$

Part 3: Shifts in Observables

We now come to the climax of this exposition. Suppose now that SMEFT represents the "true" theory, and that we wish to compute the correction to a quantity such as a cross section which has been calculated under the mistaken assumption that the SM was the correct theory: $\Delta\sigma = \sigma_{\text{SMEFT}} - \sigma_{\text{SM}}$. In addition to direct contributions from new operators, there will be an indirect contribution from the shifts of the SM parameters.

To arrive at this conclusion carefully, convince yourself that the correct cross section should be written in terms of the barred parameters, $\sigma(\bar{g}_i)$, as – after all – these parameters are the ones extant in the "true" Lagrangian. In the SM, however, it's evidently the case that both $\delta\bar{g}_i = 0$ and $\delta\hat{g}_i = 0$,[8] so one sees no issue with setting $g_i = \hat{g}_i$ and computing the cross section as $\sigma(\hat{g}_i)$. Explicitly,

$$\sigma_{\text{SMEFT}} = \sigma(\bar{g}_i) + \Delta\sigma_{\text{Direct}} \quad \text{and} \quad \sigma_{\text{SM}} = \sigma(\hat{g}_i), \tag{69}$$

and so

$$\Delta\sigma = \Delta\sigma_{\text{Direct}} + \sum_i \frac{\partial\sigma}{\partial g_i}\bigg|_{g_i=\hat{g}_i}\left(\bar{g}_i - \hat{g}_i\right)$$
$$= \Delta\sigma_{\text{Direct}} + \sum_i \frac{\partial\sigma}{\partial g_i}\bigg|_{g_i=\hat{g}_i}\delta g_i. \tag{70}$$

It is worth emphasising that Eq. (70) applies only when computing a correction to an SM prediction, which we do so in Sects. 3.1 and 3.2 of the main text. However, as in Sects. 3.3 and 3.4, it does *not* apply when one is only interested in the SMEFT prediction, σ_{SMEFT}.

[8] Of course it's not strictly true that $\delta\hat{g}_i = 0$, as there will be loop effects contributing to the screening of g_i even in the SM. This is however a separate shift to the one under consideration and it can be independently dealt with, so we do not treat it here.

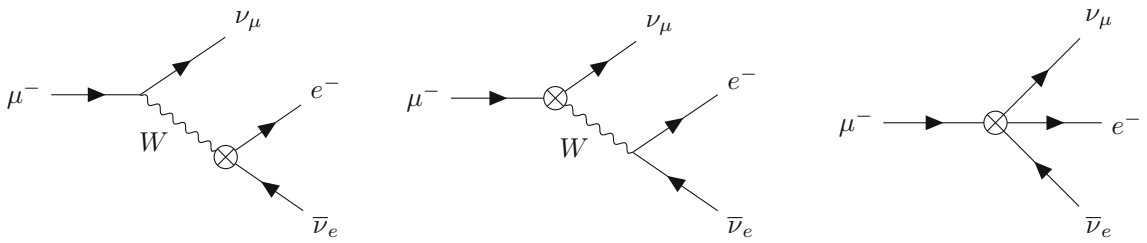

Fig. 8 Muon decay diagrams with the effective operators contributing to $\delta\hat{G}_F$, given in Eq. (5)

An explicit example

We illustrate the above procedure by working out the shift in g_{ZZh}, which appears in the SM Lagrangian as

$$\mathcal{L} \supset \frac{1}{4} g_Z^2 v Z_\mu Z^\mu h \equiv \frac{1}{2} g_{ZZh} Z_\mu Z^\mu h. \tag{71}$$

In SMEFT this becomes – with additional complications arising from the fact that the Higgs field acquires a new normalisation, see Ref. [75], and that $\mathcal{O}_{HD}$ contributes a $Z_\mu Z^\mu h$ term –

$$\begin{aligned}\mathcal{L} \supset\ & \frac{1}{4}\bar{g}_Z^2 v_T Z_\mu Z^\mu \left(1 + v_T^2 C_{H\Box} - \frac{1}{4} v_T^2 C_{HD}\right) h \\ & + C_{HD} \frac{1}{2} g_Z^2 v_T^3 Z_\mu Z^\mu h \\ =\ & \frac{1}{4} g_Z^2 v \Bigg(1 + 2\frac{\delta \bar{g}_Z}{g_Z} + \frac{\delta \bar{v}}{v} + v_T^2 C_{H\Box} \\ & + \frac{3}{4} v_T^2 C_{HD}\Bigg) Z_\mu Z^\mu h \\ \equiv\ & \frac{1}{2} \bar{g}_{ZZh} Z_\mu Z^\mu h, \end{aligned} \tag{72}$$

from which we read off

$$\begin{aligned}\frac{\delta \bar{g}_{ZZh}}{g_{ZZh}} &= 2\frac{\delta \bar{g}_Z}{g_Z} + \frac{\delta \bar{v}}{v} + v_T^2 C_{H\Box} + \frac{3}{4} v_T^2 C_{HD} \\ &= 2 c_w s_w v_T^2 C_{HWB} + v_T^2 C_{H\Box} \\ &\quad + \frac{3}{4} v_T^2 C_{HD} + \frac{\delta \bar{v}}{v}. \end{aligned} \tag{73}$$

The $\delta\hat{g}_{ZZh}$ part of the full shift depends on one's choice of input parameters; in the (α, m_Z, G_F) scheme one has

$$\hat{g}_{ZZh} = 2^{5/4} \hat{m}_Z^2 \sqrt{\hat{G}_F}, \tag{74}$$

which is a tree-level relation valid in the SM. In accordance with Eq. (66), we then have

$$\frac{\delta \hat{g}_{ZZh}}{g_{ZZh}} = \left(\frac{\delta \bar{m}_Z^2}{m_Z^2} + \frac{\delta \hat{m}_Z^2}{m_Z^2}\right) + \frac{1}{2}\left(\frac{\delta \bar{G}_F}{G_F} + \frac{\delta \hat{G}_F}{G_F}\right). \tag{75}$$

Plugging in the known shifts[9] [75]

$$\begin{aligned}\frac{\delta \bar{m}_Z^2}{m_Z^2} &= \frac{1}{2} v_T^2 C_{HD} + 2 c_w s_w v_T^2 C_{HWB} + 2\frac{\delta \bar{v}}{v}, \\ \frac{\delta \hat{m}_Z^2}{m_Z^2} &= 0, \qquad \frac{\delta \bar{G}_F}{G_F} = -2\frac{\delta \bar{v}}{v}, \end{aligned} \tag{76}$$

and leaving $\delta\hat{G}_F/G_F$ symbolic as it has a cumbersome expression (see Eq. (5)), this evaluates to

$$\frac{\delta \hat{g}_{ZZh}}{g_{ZZh}} = \frac{1}{2} v_T^2 C_{HD} + 2 c_w s_w v_T^2 C_{HWB} + \frac{\delta \bar{v}}{v} + \frac{1}{2}\frac{\delta \hat{G}_F}{G_F}. \tag{77}$$

Lastly, we bring it all together as per Eq. (68) to obtain

$$\begin{aligned}\frac{\delta g_{ZZh}}{g_{ZZh}} &= \frac{\delta \bar{g}_{ZZh}}{g_{ZZh}} - \frac{\delta \hat{g}_{ZZh}}{g_{ZZh}} \\ &= v_T^2 \left(C_{H\Box} + \frac{1}{4} C_{HD}\right) - \frac{1}{2}\frac{\delta \hat{G}_F}{G_F}, \end{aligned} \tag{78}$$

which one sees matches Eq. (28). We note that the dependence on $\delta\bar{v}$ completely cancels. This is a general trend for all shifts we consider – thus, for our purposes, the replacement $v \to v_T$ is functionally unphysical.

Appendix B: Approximate matching conditions

From `DsixTools` we numerically get the matching condition for the electromagnetic dipole operator, relevant to LFV decays:

$$\frac{C_{e\gamma,ij}\ (\mu = 5\,\text{GeV})}{\text{GeV}} \approx 150.732\, C_{eB,ij}$$

[9] One arrives at the shift $\delta\bar{G}_F$ by writing

$$\bar{G}_F = \frac{1}{\sqrt{2} v_T^2} = \frac{1}{\sqrt{2} v^2}\left(1 - 2\frac{\delta \bar{v}}{v}\right).$$

$\delta\bar{m}_Z$ is more involved, as $\bar{m}_Z^2$ additionally receives a direct contribution from $\mathcal{O}_{HD}$ and an indirect contribution from $\mathcal{O}_{HWB}$ due to the rediagonalisation of Z_μ and A_μ. Lastly, $\delta\hat{m}_Z$ is zero as there are no tree-level diagrams at order $(v/\Lambda)^2$ which contribute to the Z-boson self energy.

$$- 82.394\, C_{eW,ij} + 3.204\, C^{(3)}_{LeQu,ij33} + A_{ij}\left(C^{(3)}_{HL,ij} - 0.27353\, C^{(1)}_{HL,ij}\right), \tag{79}$$

where the Wilson coefficients on the right-hand side are evaluated at the scale $\mu = m_Z$, repeated indices do not indicate summation, and

$$A_{ij} = 10^{-3}\begin{pmatrix} - & 0.2661 & 4.4758 \\ 0.0013 & - & - \\ 0.0013 & - & - \end{pmatrix}_{ij}, \tag{80}$$

with the dashed entries being irrelevant for our purposes.

We are conscious that the scales associated with the decays of taus and muons are smaller than $\mu = 5\,\text{GeV}$. The largest contributions from RG running at lower scales can be expected to originate from QCD. The only SMEFT operator which one may a priori expect to yield a sizeable contribution to LEFT operators which involve quark fields and mix into $\mathcal{O}_{e\gamma}$ is $\mathcal{O}^{(3)}_{LeQu} = (\overline{L}\sigma_{\mu\nu}e_R)\epsilon(\overline{Q}\sigma^{\mu\nu}u_R)$. Still, this operator is not induced at 1-loop level in the Seesaw models under consideration [78–80], and it only yields a tiny sub-percent contribution to $\mathcal{O}_{e\gamma}$. Therefore, we do not expect to have missed any sizeable effects from RG running below $\mu = 5\,\text{GeV}$.[10] The same holds for the (semi-)leptonic vector operators mediating trilepton decays and $\mu - e$ conversion; we have explicitly checked that the contribution from quark operators is at most 1% in Eqs. (81) and (82) below.

For all the matching conditions listed in the following, the respective LEFT Wilson coefficient on the left-hand side is given at $\mu = 5\,\text{GeV}$, while the SMEFT Wilson coefficients entering on the right-hand side are evaluated at the scale $\mu = m_Z$. For the operators relevant to trilepton decays we find:

$$C^{VLL}_{ee,jijj} \approx -0.266\, C^{(1)}_{HL,ji} - 0.271\, C^{(3)}_{HL,ji} + 0.973\, C_{LL,jiji}, \tag{81a}$$

$$C^{VRR}_{ee,jijj} \approx 0.974\, C_{ee,jiji} + 0.235\, C_{He,ji} - 0.006\, C_{eu,ji33} + 0.003\, C_{Qe,33ji}, \tag{81b}$$

$$C^{VLR}_{ee,jijj} \approx 0.4912\, C^{(1)}_{HL,ji} + 0.4909\, C^{(3)}_{HL,ji} + 1.018\, C_{Le,jijj} - 0.012\, C_{Lu,ji33}, \quad \text{and} \tag{81c}$$

$$C^{VLR}_{ee,jiji} \approx -0.556\, C_{He,ji} + 1.018\, C_{Le,jiji} - 0.015\, C_{Qe,33ji} + 0.011\, C_{eu,ji33}. \tag{81d}$$

[10] Paraphrasing this, even if the numerical factor multiplying $C^{(3)}_{LeQu}(m_Z)$ in Eq. (79) changes appreciably upon further lowering the scale on the left-hand side to, say, $\mu = m_\mu$, $C^{(3)}_{LeQu}(m_Z)$ itself is so small for the fermionic Seesaw models that we do not expect the resulting (relative) contribution to $C_{e\gamma}(m_\mu)$ to become sizeable in any way.

For $\mu - e$ conversion the matching conditions for the vector operators are

$$C^{VLL}_{eu,1211} \approx 0.708\, C^{(1)}_{HL,12} + 0.734\, C^{(3)}_{HL,12} - 1.047\, C^{(3)}_{LQ,1211}, \tag{82a}$$

$$C^{VLR}_{eu,1211} \approx -0.3172\, C^{(1)}_{HL,12} - 0.3170\, C^{(3)}_{HL,12} + 0.984\, C_{Lu,1211}, \tag{82b}$$

$$C^{VRR}_{eu,1211} \approx -0.321\, C_{He,12} + 0.008\, C_{eu,1233} - 0.005\, C_{Qe,3312}, \tag{82c}$$

$$C^{VLR}_{ue,1112} \approx 0.696\, C_{He,12} + 0.017\, C_{Qe,3312} - 0.014\, C_{eu,1233}, \tag{82d}$$

$$C^{VLL}_{ed,1211} \approx -0.856\, C^{(1)}_{HL,12} - 0.864\, C^{(3)}_{HL,12} + 0.987\, C^{(3)}_{LQ,1211}, \tag{82e}$$

$$C^{VLR}_{ed,1211} \approx 0.1617\, C^{(1)}_{HL,12} + 0.1615\, C^{(3)}_{HL,12} + 1.006\, C_{Ld,1211}, \tag{82f}$$

$$C^{VRR}_{ed,1211} \approx 0.158\, C_{He,12} - 0.004\, C_{eu,1233} + 0.002\, C_{Qe,3312}, \quad \text{and} \tag{82g}$$

$$C^{VLR}_{de,1112} \approx -0.867\, C_{He,12} - 0.020\, C_{Qe,3312} + 0.018\, C_{eu,1233}. \tag{82h}$$

References

1. G. Aad et al., Observation of a new particle in the search for the Standard Model Higgs boson with the ATLAS detector at the LHC. Phys. Lett. B **716**, 1–29 (2012). https://doi.org/10.1016/j.physletb.2012.08.020. arXiv:1207.7214 [hep-ex]
2. S. Chatrchyan et al., Observation of a new boson at a mass of 125 GeV with the CMS experiment at the LHC. Phys. Lett. B **716**, 30–61 (2012). https://doi.org/10.1016/j.physletb.2012.08.021. arXiv:1207.7235 [hep-ex]
3. S. Dawson et al., Report of the Topical Group on Higgs Physics for Snowmass 2021: The Case for Precision Higgs Physics. (2022). arXiv:2209.07510 [hep-ph]
4. M. Ahmad et al., CEPC-SPPC Preliminary Conceptual Design Report. 1. Physics and Detector. (2015). IHEP-CEPC-DR-2015-01
5. J. B. Guimarães da Costa et al., [CEPC Study Group], CEPC Conceptual Design Report: Volume 2 - Physics & Detector (2018) arXiv:1811.10545 [hep-ex]
6. H. Cheng et al., CEPC Physics Study Group], The Physics potential of the CEPC. Prepared for the US Snowmass Community Planning Exercise (Snowmass 2021). arXiv:2205.08553 [hep-ph]
7. H. Baer et al., The international linear collider technical design report–volume 2: physics (2013). arXiv:1306.6352 [hep-ph]
8. D. M. Asner et al., ILC Higgs white paper, (2013). arXiv:1310.0763 [hep-ph]
9. P. Bambade et.al., The international linear collider: a global project (2019). arXiv:1903.01629 [hep-ex]
10. A. Aryshev et al., [ILC International Development Team], The international linear collider: report to Snowmass 2021 (2022). arXiv:2203.07622 [physics.acc-ph]

11. M. Bicer et al., First look at the physics case of TLEP. JHEP **01**, 164 (2014). https://doi.org/10.1007/JHEP01(2014)164. arXiv:1308.6176 [hep-ex]
12. A. Pyarelal, H. Song, S. Su, FCC-ee: the lepton collider: future circular collider conceptual design report volume 2. Eur. Phys. J. Spec. Top. (2019). https://doi.org/10.1140/epjst/e2019-900045-4
13. I. Agapov et al., Future circular lepton collider FCC-ee: overview and status, (2022). arXiv:2203.08310 [physics.acc-ph]
14. G. Bernardi et al., The future circular collider: a summary for the US 2021 Snowmass process (2022). arXiv:2203.06520 [hep-ex]
15. P. Lebrun, L. Linssen, A. Lucaci-Timoce, D. Schulte, F. Simon, S. Stapnes, N. Toge, H. Weerts, J. Wells, The CLIC Programme: towards a staged e^+e^- linear collider exploring the Terascale: CLIC conceptual design report (2012). https://doi.org/10.5170/CERN-2012-005. arXiv:1209.2543 [physics.ins-det]
16. J. de Blas et al., The CLIC potential for new physics **3/2018** (2018). https://doi.org/10.23731/CYRM-2018-003. arXiv:1812.02093 [hep-ph]
17. T.K. Charles et al., The compact linear collider (CLIC)—2018 summary report **2/2018** (2018). https://doi.org/10.23731/CYRM-2018-002. arXiv:1812.06018 [physics.acc-ph]
18. M. Bai et al., C^3: a "'Cool" route to the Higgs boson and beyond, (2021). arXiv:2110.15800 [hep-ex]
19. E. A. Nanni et al., C^3 demonstration research and development plan (2022). arXiv:2203.09076 [physics.acc-ph]
20. S. Dasu et al., Strategy for understanding the Higgs physics: the cool copper collider (2022). arXiv:2203.07646 [hep-ex]
21. E. Aslanides et al., Charting the European course to the high-energy frontier (2019). arXiv:1912.13466 [hep-ex]
22. Y. Fukuda et al., Evidence for oscillation of atmospheric neutrinos. Phys. Rev. Lett. **81**, 1562–1567 (1998). https://doi.org/10.1103/PhysRevLett.81.1562. arXiv:hep-ex/9807003
23. Q.R. Ahmad et al., Measurement of the rate of $\nu_e+d \rightarrow p+p+e^-$ interactions produced by ^{8}B solar neutrinos at the Sudbury Neutrino Observatory. Phys. Rev. Lett. **87**, 071301 (2001). https://doi.org/10.1103/PhysRevLett.87.071301. arXiv:nucl-ex/0106015
24. Q.R. Ahmad et al., Direct evidence for neutrino flavor transformation from neutral current interactions in the Sudbury Neutrino Observatory. Phys. Rev. Lett. **89**, 011301 (2002). https://doi.org/10.1103/PhysRevLett.89.011301. arXiv:nucl-ex/0204008
25. F. del Aguila, J.A. Aguilar-Saavedra, A. Martinez de la Ossa, D. Meloni, Flavor and polarisation in heavy neutrino production at e^+e^- colliders. Phys. Lett. B, **613**, 170–180 (2005). https://doi.org/10.1016/j.j.physletb.2005.03.054. arXiv:hep-ph/0502189
26. F. del Aguila, J.A. Aguilar-Saavedra, $\ell W \nu$ production at CLIC: a window to TeV scale non-decoupled neutrinos. JHEP **05**, 026 (2005). https://doi.org/10.1088/1126-6708/2005/05/026. arXiv:hep-ph/0503026
27. S. Antusch, O. Fischer, Testing sterile neutrino extensions of the Standard Model at future lepton colliders. JHEP **05**, 053 (2015). https://doi.org/10.1007/JHEP05(2015)053. arXiv:1502.05915 [hep-ph]
28. S. Antusch, E. Cazzato, O. Fischer, Higgs production from sterile neutrinos at future lepton colliders. JHEP **04**, 189 (2016). https://doi.org/10.1007/JHEP04(2016)189. arXiv:1512.06035 [hep-ph]
29. S. Antusch, E. Cazzato, O. Fischer, Displaced vertex searches for sterile neutrinos at future lepton colliders. JHEP **12**, 007 (2016). https://doi.org/10.1007/JHEP12(2016)007. arXiv:1604.02420 [hep-ph]
30. Y. Zhang, B. Zhang, A potential scenario for Majorana neutrino detection at future lepton colliders. JHEP **02**, 175 (2019). https://doi.org/10.1007/JHEP02(2019)175. arXiv:1805.09520 [hep-ph]
31. A. Das, S. Jana, S. Mandal, S. Nandi, Probing right handed neutrinos at the LHeC and lepton colliders using fat jet signatures. Phys. Rev. D **99**(5), 055030 (2019). https://doi.org/10.1103/PhysRevD.99.055030. arXiv:1811.04291 [hep-ph]
32. D. Barducci, E. Bertuzzo, A. Caputo, P. Hernandez, B. Mele, The see-saw portal at future Higgs Factories. JHEP **03**, 117 (2021). https://doi.org/10.1007/JHEP03(2021)117. arXiv:2011.04725 [hep-ph]
33. Y. Gao, K. Wang, Heavy neutrino searches via same-sign lepton pairs at a Higgs boson factory. Phys. Rev. D **105**(7), 076005 (2022). https://doi.org/10.1103/PhysRevD.105.076005. arXiv:2102.12826 [hep-ph]
34. F.F. Deppisch, P.S. Bhupal Dev, A. Pilaftsis, Neutrinos and collider physics. New J. Phys. **17**(7), 075019 (2015). https://doi.org/10.1088/1367-2630/17/7/075019. arXiv:1502.06541 [hep-ph]
35. Y. Cai, T. Han, T. Li, R. Ruiz, Lepton number violation: Seesaw models and their collider tests. Front. Phys. **6**, 40 (2018). https://doi.org/10.3389/fphy.2018.00040. arXiv:1711.02180 [hep-ph]
36. A. Das, Searching for the minimal Seesaw models at the LHC and beyond. Adv. High Energy Phys. **2018**, 9785318 (2018). https://doi.org/10.1155/2018/9785318. arXiv:1803.10940 [hep-ph]
37. A. M. Abdullahi et al. The present and future status of heavy neutral leptons. J. Phys. G **50** (2), 020501 (2023). https://doi.org/10.1088/1361-6471/ac98f9. arXiv:2203.08039 [hep-ph]
38. A. Das, S. Mandal, Bounds on the triplet fermions in type-III seesaw and implications for collider searches. Nucl. Phys. B **966**, 115374 (2021). https://doi.org/10.1016/j.nuclphysb.2021.115374. arXiv:2006.04123 [hep-ph]
39. C. A. Argüelles et al., Snowmass white paper: beyond the standard model effects on neutrino flavor: Submitted to the proceedings of the US community study on the future of particle physics (Snowmass 2021), Eur. Phys. J. C **83**(1), 15 (2023). https://doi.org/10.1140/epjc/s10052-022-11049-7. arXiv:2203.10811 [hep-ph]
40. S.-F. Ge, H.-J. He, R.-Q. Xiao, Probing new physics scales from Higgs and electroweak observables at e^+e^- Higgs factory. JHEP **10**, 007 (2016). https://doi.org/10.1007/JHEP10(2016)007. arXiv:1603.03385 [hep-ph]
41. J. Baglio, C. Weiland, The triple Higgs coupling: a new probe of low-scale seesaw models. JHEP **04**, 038 (2017). https://doi.org/10.1007/JHEP04(2017)038. arXiv:1612.06403 [hep-ph]
42. J. Baglio, C. Weiland, Heavy neutrino impact on the triple Higgs coupling. Phys. Rev. D **94**(1), 013002 (2016). https://doi.org/10.1103/PhysRevD.94.013002. arXiv:1603.00879 [hep-ph]
43. P. Minkowski, $\mu \rightarrow e\gamma$ at a rate of one out of 10^9 muon decays? Phys. Lett. **67B**, 421–428 (1977). https://doi.org/10.1016/0370-2693(77)90435-X
44. T. Yanagida, Horizontal gauge symmetry and masses of neutrinos. Conf. Proc. C **7902131**, 95–99 (1979)
45. M. Gell-Mann, P. Ramond, R. Slansky, Complex spinors and unified theories, Conf. Proc. C **790927**, 315–321 (1979) arXiv:1306.4669 [hep-th]
46. S.L. Glashow, *Quarks and Leptons, Cargèse 1979* (Plenum Press, New York, 1980), p.720
47. R.N. Mohapatra, G. Senjanovic, Neutrino mass and spontaneous parity nonconservation. Phys. Rev. Lett. **44**, 912 (1980). https://doi.org/10.1103/PhysRevLett.44.912
48. R. Foot, H. Lew, X.G. He, G.C. Joshi, Seesaw neutrino masses induced by a triplet of leptons. Z. Phys. C **44**, 441 (1989). https://doi.org/10.1007/BF01415558
49. A. Freitas, Q. Song, Two-loop electroweak corrections with fermion loops to $e^+e^- \rightarrow ZH$. Phys. Rev. Lett. **130**(3), 031801 (2023). https://doi.org/10.1103/PhysRevLett.130.031801. arXiv:2209.07612 [hep-ph]
50. X. Chen, X. Guan, C. Q. He, Z. Li, X. Liu, Y. Q. Ma, Complete two-loop electroweak corrections to $e^+e^- \rightarrow HZ$ (2022). arXiv:2209.14953 [hep-ph]
51. J. Fleischer, F. Jegerlehner, Radiative corrections to Higgs production by $e^+e^- \rightarrow Zh$ in the Weinberg–Salam model. Nucl. Phys. B **216**(2), 469–492 (1983). https://doi.org/10.1016/0550-3213(83)90296-1

52. B.A. Kniehl, Radiative corrections for associated ZH production at future e^+e^- colliders. Zeitschrift für Physik C Particles and Fields **55**, 605–618 (1991)
53. A. Denner, J. Kublbeck, R. Mertig, M. Bohm, Electroweak radiative corrections to $e^+e^- \to Zh$. Z. Phys. C **56**, 261–272 (1992). https://doi.org/10.1007/BF01555523
54. S. Bondarenko, Y. Dydyshka, L. Kalinovskaya, L. Rumyantsev, R. Sadykov, V. Yermolchyk, One-loop electroweak radiative corrections to polarized $e^+e^- \to ZH$. Phys. Rev. D **100**(7), 073002 (2019). https://doi.org/10.1103/PhysRevD.100.073002. arXiv:1812.10965 [hep-ph]
55. Y. Gong, Z. Li, X. Xu, L.L. Yang, X. Zhao, Mixed QCD-EW corrections for Higgs boson production at e^+e^- colliders. Phys. Rev. D **95**(9), 093003 (2017). https://doi.org/10.1103/PhysRevD.95.093003. arXiv:1609.03955 [hep-ph]
56. Q.-F. Sun, F. Feng, Y. Jia, W.-L. Sang, Mixed electroweak-QCD corrections to $e^+e^- \to ZH$ at Higgs factories. Phys. Rev. D **96**(5), 051301 (2017). https://doi.org/10.1103/PhysRevD.96.051301. arXiv:1609.03995 [hep-ph]
57. W. Chen, F. Feng, Y. Jia, W.-L. Sang, Mixed electroweak-QCD corrections to $e^+e^- \to \mu^+\mu^- H$ at CEPC with finite-width effect. Chin. Phys. C **43**(1), 013108 (2019). https://doi.org/10.1088/1674-1137/43/1/013108. arXiv:1811.05453 [hep-ph]
58. H. Abramowicz et al., Higgs physics at the CLIC electron–positron linear collider. Eur. Phys. J. C **77**(7), 475 (2017). https://doi.org/10.1140/epjc/s10052-017-4968-5. arXiv:1608.07538 [hep-ex]
59. J. Kersten, A.Y. Smirnov, Right-handed neutrinos at CERN LHC and the mechanism of neutrino mass generation. Phys. Rev. D **76**, 073005 (2007). https://doi.org/10.1103/PhysRevD.76.073005. arXiv:0705.3221 [hep-ph]
60. M. Drewes, J. Klarić, P. Klose, On lepton number violation in heavy neutrino decays at colliders. JHEP **11**, 032 (2019). https://doi.org/10.1007/JHEP11(2019)032. arXiv:1907.13034 [hep-ph]
61. A. Abada, P. Escribano, X. Marcano, G. Piazza, Collider searches for heavy neutral leptons: beyond simplified scenarios. Eur. Phys. J. C **82**(11), 1030 (2022). https://doi.org/10.1140/epjc/s10052-022-11011-7. arXiv:2208.13882 [hep-ph]
62. D. Wyler, L. Wolfenstein, Massless neutrinos in left-right symmetric models. Nucl. Phys. B **218**, 205–214 (1983). https://doi.org/10.1016/0550-3213(83)90482-0
63. J. Bernabeu, A. Santamaria, J. Vidal, A. Mendez, J.W.F. Valle, Lepton flavor nonconservation at high-energies in a superstring inspired standard model. Phys. Lett. B **187**, 303–308 (1987). https://doi.org/10.1016/0370-2693(87)91100-2
64. G.C. Branco, W. Grimus, L. Lavoura, The seesaw mechanism in the presence of a conserved lepton number. Nucl. Phys. B **312**, 492–508 (1989). https://doi.org/10.1016/0550-3213(89)90304-0
65. D. Tommasini, G. Barenboim, J. Bernabeu, C. Jarlskog, Non-decoupling of heavy neutrinos and lepton flavor violation. Nucl. Phys. B **444**, 451–467 (1995). https://doi.org/10.1016/0550-3213(95)00201-3. arXiv:hep-ph/9503228
66. A. Pilaftsis, Resonant tau-leptogenesis with observable lepton number violation. Phys. Rev. Lett. **95**, 081602 (2005). https://doi.org/10.1103/PhysRevLett.95.081602. arXiv:hep-ph/0408103
67. A. Pilaftsis, T.E.J. Underwood, Electroweak-scale resonant leptogenesis. Phys. Rev. D **72**, 113001 (2005). https://doi.org/10.1103/PhysRevD.72.113001. arXiv:hep-ph/0506107
68. M. Shaposhnikov, A possible symmetry of the νMSM. Nucl. Phys. B **763**, 49–59 (2007). https://doi.org/10.1016/j.nuclphysb.2006.11.003. arXiv:hep-ph/0605047
69. A. Abada, C. Biggio, F. Bonnet, M.B. Gavela, T. Hambye, Low energy effects of neutrino masses. JHEP **12**, 061 (2007). https://doi.org/10.1088/1126-6708/2007/12/061. arXiv:0707.4058 [hep-ph]
70. M.B. Gavela, T. Hambye, D. Hernandez, P. Hernandez, Minimal flavour seesaw models. JHEP **09**, 038 (2009). https://doi.org/10.1088/1126-6708/2009/09/038. arXiv:0906.1461 [hep-ph]
71. O.J.P. Eboli, J. Gonzalez-Fraile, M.C. Gonzalez-Garcia, Neutrino masses at LHC: minimal lepton flavour violation in type-III see-saw. JHEP **12**, 009 (2011). https://doi.org/10.1007/JHEP12(2011)009. arXiv:1108.0661 [hep-ph]
72. E. Fernandez-Martinez, J. Hernandez-Garcia, J. Lopez-Pavon, M. Lucente, Loop level constraints on Seesaw neutrino mixing. JHEP **10**, 130 (2015). https://doi.org/10.1007/JHEP10(2015)130. arXiv:1508.03051 [hep-ph]
73. B. Grzadkowski, M. Iskrzynski, M. Misiak, J. Rosiek, Dimension-six terms in the standard model Lagrangian. JHEP **10**, 085 (2010). https://doi.org/10.1007/JHEP10(2010)085. arXiv:1008.4884 [hep-ph]
74. L. Berthier, M. Trott, Towards consistent electroweak precision data constraints in the SMEFT. JHEP **05**, 024 (2015). https://doi.org/10.1007/JHEP05(2015)024. arXiv:1502.02570 [hep-ph]
75. R. Alonso, E.E. Jenkins, A.V. Manohar, M. Trott, Renormalization group evolution of the standard model dimension six operators III: gauge coupling dependence and phenomenology. JHEP **04**, 159 (2014). https://doi.org/10.1007/JHEP04(2014)159. arXiv:1312.2014 [hep-ph]
76. E.E. Jenkins, A.V. Manohar, P. Stoffer, Low-energy effective field theory below the electroweak scale: operators and matching. JHEP **03**, 016 (2018). https://doi.org/10.1007/JHEP03(2018)016. arXiv:1709.04486 [hep-ph]
77. A. Celis, J. Fuentes-Martin, A. Vicente, J. Virto, Dsix-Tools: the standard model effective field theory toolkit. Eur. Phys. J. C **77**(6), 405 (2017). https://doi.org/10.1140/epjc/s10052-017-4967-6. arXiv:1704.04504 [hep-ph]
78. Y. Du, X.-X. Li, J.-H. Yu, Neutrino seesaw models at one-loop matching: discrimination by effective operators. JHEP **09**, 207 (2022). https://doi.org/10.1007/JHEP09(2022)207. arXiv:2201.04646 [hep-ph]
79. D. Zhang, S. Zhou, Complete one-loop matching of the type-I seesaw model onto the Standard Model effective field theory. JHEP **09**, 163 (2021). https://doi.org/10.1007/JHEP09(2021)163. arXiv:2107.12133 [hep-ph]
80. R. Coy, M. Frigerio, Effective comparison of neutrino-mass models. Phys. Rev. D **105**(11), 115041 (2022). https://doi.org/10.1103/PhysRevD.105.115041. arXiv:2110.09126 [hep-ph]
81. P.B. Pal, Dirac, Majorana, and Weyl fermions. Am. J. Phys. **79**(5), 485–498 (2011). https://doi.org/10.1119/1.3549729. arXiv:1006.1718 [hep-ph]
82. C. Biggio, E. Fernandez-Martinez, M. Filaci, J. Hernandez-Garcia, J. Lopez-Pavon, Global bounds on the type-III seesaw. JHEP **05**, 022 (2020). https://doi.org/10.1007/JHEP05(2020)022. arXiv:1911.11790 [hep-ph]
83. R.N. Mohapatra, Mechanism for understanding small neutrino mass in superstring theories. Phys. Rev. Lett. **56**, 561–563 (1986). https://doi.org/10.1103/PhysRevLett.56.561
84. R.N. Mohapatra, J.W.F. Valle, Neutrino mass and baryon number nonconservation in superstring models. Phys. Rev. D **34**, 1642 (1986). https://doi.org/10.1103/PhysRevD.34.1642
85. E.K. Akhmedov, M. Lindner, E. Schnapka, J.W.F. Valle, Left-right symmetry breaking in NJL approach. Phys. Lett. B **368**, 270–280 (1996). https://doi.org/10.1016/0370-2693(95)01504-3. arXiv:hep-ph/9507275
86. E.K. Akhmedov, M. Lindner, E. Schnapka, J.W.F. Valle, Dynamical left-right symmetry breaking. Phys. Rev. D **53**, 2752–2780 (1996). https://doi.org/10.1103/PhysRevD.53.2752. arXiv:hep-ph/9509255
87. A. Donini, P. Hernandez, J. Lopez-Pavon, M. Maltoni, T. Schwetz, The minimal 3+2 neutrino model versus oscillation anomalies.

JHEP **07**, 161 (2012). https://doi.org/10.1007/JHEP07(2012)161. arXiv:1205.5230 [hep-ph]
88. A.M. Sirunyan et al., Search for heavy neutral leptons in events with three charged leptons in proton-proton collisions at $\sqrt{s} =$ 13 TeV. Phys. Rev. Lett. **120**(22), 221801 (2018). https://doi.org/10.1103/PhysRevLett.120.221801. arXiv:1802.02965 [hep-ex]
89. CMS Collaboration, Probing heavy Majorana neutrinos and the Weinberg operator through vector boson fusion processes in proton–proton collisions at $\sqrt{s} =$ 13 TeV (2022). arXiv:2206.08956 [hep-ex]
90. G. Aad et al., Search for type-III seesaw heavy leptons in leptonic final states in pp collisions at $\sqrt{s} =$ 13 TeV with the ATLAS detector. Eur. Phys. J. C **82**(11), 988 (2022). https://doi.org/10.1140/epjc/s10052-022-10785-0. arXiv:2202.02039 [hep-ex]
91. B.A. Kniehl, A. Pilaftsis, Quantum effects on Higgs-boson production and decay due to Majorana neutrinos. Nucl. Phys. B **424**(1), 18–38 (1994). https://doi.org/10.1016/0550-3213(94)90086-8. arXiv:hep-ph/9402314
92. N. Craig, M. Farina, M. McCullough, M. Perelstein, Precision Higgsstrahlung as a probe of new physics. JHEP **03**, 146 (2015). https://doi.org/10.1007/JHEP03(2015)146. arXiv:1411.0676 [hep-ph]
93. J. Yan, S. Watanuki, K. Fujii, A. Ishikawa, D. Jeans, J. Strube, J. Tian, H. Yamamoto, Measurement of the Higgs boson mass and $e^+e^- \to ZH$ cross section using $Z \to \mu^+\mu^-$ and $Z \to e^+e^-$ at the ILC. Phys. Rev. D **94**(11), 113002 (2016). https://doi.org/10.1103/PhysRevD.94.113002. arXiv:1604.07524 [hep-ex]. [Erratum: Phys. Rev. D **103**, 099903 (2021)]
94. M. Thomson, Model-independent measurement of the $e^+e^- \to$ HZ cross section at a future e^+e^- linear collider using hadronic Z decays. Eur. Phys. J. C **76**(2), 72 (2016). https://doi.org/10.1140/epjc/s10052-016-3911-5. arXiv:1509.02853 [hep-ex]
95. A. Miyamoto, A measurement of the total cross section of σ_{Zh} at a future e^+e^- collider using the hadronic decay mode of Z (2013). arXiv:1311.2248 [hep-ex]
96. J. de Blas, M. Ciuchini, E. Franco, A. Goncalves, S. Mishima, M. Pierini, L. Reina, L. Silvestrini, Global analysis of electroweak data in the Standard Model. Phys. Rev. D **106**(3), 033003 (2022). https://doi.org/10.1103/PhysRevD.106.033003. arXiv:2112.07274 [hep-ph]
97. S. Schael et al., Precision electroweak measurements on the Z resonance. Phys. Rep. **427**, 257–454 (2006). https://doi.org/10.1016/j.physrep.2005.12.006. arXiv:hep-ex/0509008
98. R.L. Workman et al., [Particle Data Group], Review of particle physics. PTEP **2022**, 083C01 (2022). https://doi.org/10.1093/ptep/ptac097
99. T. Aaltonen et al., High-precision measurement of the W boson mass with the CDF II detector. Science **376**(6589), 170–176 (2022). https://doi.org/10.1126/science.abk1781
100. A. Pich, Challenges for tau physics at the TeraZ. Eur. Phys. J. Plus **136**(11), 1117 (2021). https://doi.org/10.1140/epjp/s13360-021-02077-5. arXiv:2012.07099 [hep-ph]
101. C.-Y. Seng, D. Galviz, M. Gorchtein, U.-G. Meißner, Complete theory of radiative corrections to $K_{\ell 3}$ decays and the V_{us} update. JHEP **07**, 071 (2022). https://doi.org/10.1007/JHEP07(2022)071. arXiv:2203.05217 [hep-ph]
102. A. Crivellin, M. Hoferichter, β Decays as sensitive probes of lepton flavor universality. Phys. Rev. Lett. **125**(11), 111801 (2020). https://doi.org/10.1103/PhysRevLett.125.111801. arXiv:2002.07184 [hep-ph]
103. D. Bryman, V. Cirigliano, A. Crivellin, G. Inguglia, Testing lepton flavor universality with pion, kaon, tau, and beta decays (2021). https://doi.org/10.1146/annurev-nucl-110121-051223. arXiv:2111.05338 [hep-ph]
104. A.M. Baldini et al., Search for the lepton flavour violating decay $\mu^+ \to e^+\gamma$ with the full dataset of the MEG experiment. Eur. Phys. J. C **76**(8), 434 (2016). https://doi.org/10.1140/epjc/s10052-016-4271-x. arXiv:1605.05081 [hep-ex]
105. A.M. Baldini et al., The search for $\mu^+ \to e^+\gamma$ with 10^{-14} sensitivity: the upgrade of the MEG experiment. Symmetry **13**(9), 1591 (2021). https://doi.org/10.3390/sym13091591. arXiv:2107.10767 [hep-ex]
106. U. Bellgardt et al., Search for the decay $\mu^+ \to e^+e^+e^-$. Nucl. Phys. B **299**, 1–6 (1988). https://doi.org/10.1016/0550-3213(88)90462-2
107. A. Blondel et al., Research proposal for an experiment to search for the decay $\mu \to eee$ (2013). arXiv:1301.6113 [physics.ins-det]
108. W.H. Bertl et al., A search for muon to electron conversion in muonic gold. Eur. Phys. J. C **47**, 337–346 (2006). https://doi.org/10.1140/epjc/s2006-02582-x
109. R. Abramishvili et al., COMET phase-I technical design report. PTEP **2020**(3), 033C01 (2020). https://doi.org/10.1093/ptep/ptz125. arXiv:1812.09018 [physics.ins-det]
110. M.T. Hedges, The Mu2e experiment—searching for charged lepton flavor violation. Nucl. Instrum. Methods A **1045**, 167589 (2023). https://doi.org/10.1016/j.nima.2022.167589. arXiv:2210.14317 [hep-ex]
111. P. Wintz, Results of the SINDRUM-II experiment. Conf. Proc. C **980420**, 534–546 (1998)
112. Y. Kuno, PRISM/PRIME. Nucl. Phys. B Proc. Suppl. **149**, 376–378 (2005). https://doi.org/10.1016/j.nuclphysbps.2005.05.073
113. W. Honecker et al., Improved limit on the branching ratio of $\mu \to e$ conversion on lead. Phys. Rev. Lett. **76**, 200–203 (1996). https://doi.org/10.1103/PhysRevLett.76.200
114. A. Badertscher et al., New upper limits for muon—electron conversion in sulfur. Lett. Nuovo Cim. **28**, 401–408 (1980). https://doi.org/10.1007/BF02776193
115. B. Aubert et al., Searches for lepton flavor violation in the decays $\tau^\pm \to e^\pm\gamma$ and $\tau^\pm \to \mu^\pm\gamma$. Phys. Rev. Lett. **104**, 021802 (2010). https://doi.org/10.1103/PhysRevLett.104.021802. arXiv:0908.2381 [hep-ex]
116. S. Banerjee et al., Snowmass 2021 white paper: charged lepton flavor violation in the tau sector, in *2022 Snowmass Summer Study* (2022). arXiv:2203.14919 [hep-ph]
117. K. Hayasaka et al., Search for lepton flavor violating tau decays into three leptons with 719 million produced $\tau^+\tau^-$ pairs. Phys. Lett. B **687**, 139–143 (2010). https://doi.org/10.1016/j.physletb.2010.03.037. arXiv:1001.3221 [hep-ex]
118. A. Crivellin, F. Kirk, C.A. Manzari, Comprehensive analysis of charged lepton flavour violation in the symmetry protected type-I seesaw. JHEP **12**, 031 (2022). https://doi.org/10.1007/JHEP12(2022)031. arXiv:2208.00020 [hep-ph]
119. Y. Kuno, Y. Okada, Muon decay and physics beyond the standard model. Rev. Mod. Phys. **73**, 151–202 (2001). https://doi.org/10.1103/RevModPhys.73.151. arXiv:hep-ph/9909265
120. L. Calibbi, X. Marcano, J. Roy, Z lepton flavour violation as a probe for new physics at future e^+e^- colliders. Eur. Phys. J. C **81**(12), 1054 (2021). https://doi.org/10.1140/epjc/s10052-021-09777-3. arXiv:2107.10273 [hep-ph]
121. A. Brignole, A. Rossi, Anatomy and phenomenology of mu-tau lepton flavor violation in the MSSM. Nucl. Phys. B **701**, 3–53 (2004). https://doi.org/10.1016/j.nuclphysb.2004.08.037. arXiv:hep-ph/0404211
122. R. Kitano, M. Koike, Y. Okada, Detailed calculation of lepton flavor violating muon electron conversion rate for various nuclei. Phys. Rev. D **66**, 096002 (2002). https://doi.org/10.1103/PhysRevD.76.059902. arXiv:hep-ph/0203110. [Erratum: Phys. Rev. D **76**, 059902 (2007)]
123. V. Cirigliano, R. Kitano, Y. Okada, P. Tuzon, On the model discriminating power of $\mu \to e$ conversion in nuclei. Phys. Rev. D **80**, 013002 (2009). https://doi.org/10.1103/PhysRevD.80.013002. arXiv:0904.0957 [hep-ph]

124. T. Suzuki, D.F. Measday, J.P. Roalsvig, Total nuclear capture rates for negative muons. Phys. Rev. C **35**, 2212–2224 (1987). https://doi.org/10.1103/PhysRevC.35.2212
125. R. Alonso, M. Dhen, M.B. Gavela, T. Hambye, Muon conversion to electron in nuclei in type-I seesaw models. JHEP **01**, 118 (2013). https://doi.org/10.1007/JHEP01(2013)118. arXiv:1209.2679 [hep-ph]
126. N. Craig, J. Gu, Z. Liu, K. Wang, Beyond Higgs couplings: probing the Higgs with angular observables at future e^+e^- colliders. JHEP **03**, 050 (2016). https://doi.org/10.1007/JHEP03(2016)050. arXiv:1512.06877 [hep-ph]
127. J. Ellis, TikZ-Feynman: Feynman diagrams with TikZ. Comput. Phys. Commun. **210**, 103–123 (2017). https://doi.org/10.1016/j.cpc.2016.08.019. arXiv:1601.05437 [hep-ph]